phosphorylated cortactin was shown to associate with Fyn kinase in metastatic murine melanoma in our previous study (16). However, how cortactin phosphorylation affects intercellular signaling pathways for cell dynamics control and other functions is not understood.

It has been demonstrated that cell motility involves coordination of multiple signaling pathways regulating cell-substrate adhesion or actin polymerization (17, 18). A docking protein, p130Cas (Crk-associated substrate) is one of the key components of integrin-mediated signaling pathways, which conducts cell migration and actin filament reorganization in a tyrosine phosphorylation-dependent manner (19, 20). The C-terminal domain of p130Cas has both consensus SH3 and SH2 domains binding sites for SFKs, which are mainly responsible for the phosphorylation of p130Cas (21).

In this study, we investigated the role of cortactin in human gastric cancer cell lines using RNA interference (RNAi) technique, and discovered that knockdown of cortactin led to suppression of cell migration of the cells in which phosphorylation of cortactin is at basal level, while it increased cell migration of the cells in which cortactin is highly phosphorylated. It was also observed that knockdown of cortactin resulted in enhancement of cell motility of breast cancer cell line MCF7 in which phosphorylation level of cortactin was elevated by exogenously introduced Fyn kinase. In both cases, marked elevation in tyrosine phosphorylation of p130Cas was specifically and consistently observed by knockdown of hyperphosphorylated cortactin. We propose that tyrosine phosphorylation of cortactin may function as a molecular switch buffering the change in cell motility.

Results:

Effect on cortactin knockdown on cell migration of gastric cancer cells

Levels of tyrosine phosphorylation of cortactin were examined in human gastric cancer cell lines HSC57, HSC44As3, HSC44PE and HSC58As9 established in NCCRI, Japan (22), along with a breast carcinoma cell line MCF7 which possesses amplification of cortactin gene, *EMSI*(2). Expression of total cortactin was at similar levels (Figure 1A, lower panel), while there was a significant difference in tyrosine phosphorylation among these cell lines (Figure 1A, upper panel). HSC57, HSC44As3 and MCF7 cells exhibited a low level of tyrosine phosphorylation of cortactin, whereas HSC44PE and HSC58As9 showed hyperphosphorylation of cortactin as also indicated by the ratio of tyrosine phosphorylated cortactin to total cortactin (Figure 1A).

We knocked down cortactin expression by small interfering RNA (siRNA) to investigate the function of cortactin in the regulation of cell motility in various cancer cells using Transwell assay. It was confirmed by immunoblotting that more than 80% of cortactin expression was down-regulated at 72 hours after initiation of siRNA treatment (Figure 1B).

Interestingly, knockdown of cortactin increased cell migration in HSC44PE and HSC58As9 cells with hyperphosphorylated cortactin, while it impaired cell motility in HSC57, Hsc44As3 and MCF7 cells with a low level of phosphorylated cortactin (Figure 1C). Essentially similar effect on cell migration was seen by another siRNA, cort-siRNA2 (data not shown). To further confirm the migration promoting effect of cortactin siRNA in HSC44PE cells, we expressed mouse cortactin (mcort-WT) which is well conserved to human cortactin by the retrovirus vector (4), along with the mutant mouse cortactin (mcort-Mut) which lacks all 3 putative tyrosine phosphorylation sites by exchanging tyrosine residues 421, 466 and 482 to phenylalanine (F421F466F482). Wild type cortactin but not the mutant cortactin could block the elevation of cell migration induced by siRNA of cortactin in HSC44PE cells suggesting that cortactin is actually suppressing migration of HSC44PE cells in a tyrosine phosphorylation-dependent manner. These results indicate that cortactin might differentially exert negatively- and positively- regulating functions in cell migration depending on its tyrosine phosphorylation.

Cortactin was originally identified as a substrate of SFKs. Among SFKs expressing in solid tumor cells, Fyn kinase was shown to play central roles of in the tyrosine phosphorylation of cortactin in murine melanoma cells in our previous study (16). Treatment by a Src family specific inhibitor PP2 significantly reduced tyrosine phosphorylation of cortactin in HSC44PE cells (Supplementary Figure A), suggesting that Src family kinases are actually responsible for tyrosine phosphorylation of cortactin in HSC44PE cells. Relatively high expression of Fyn kinase along with stable association between Fyn and cortactin was observed in HSC44PE cells (Supplementary Figure B & C), suggesting the possibility that Fyn kinase is involved in hyperphosphorylation of cortactin in HSC44PE cells.

Knockdown of cortactin enhanced tyrosine phosphorylation of p130Cas in the cells with hyperphosphorylation of cortactin

By knockdown of cortactin, tyrosine phosphorylation of a 125~130KDa protein was remarkably enhanced in HSC44PE cells but not in HSC57 cells (Figure 2A). In HSC44PE cells treated with cortactin siRNA, dramatically increased tyrosine phosphorylation of p130Cas was observed using phospho-specific antibody of p130Cas (P-Cas460Y) at the exactly same position where the 125~130KDa protein detected by 4G10 (Figure 2B), while anti-phospho-FAK (Tyr397) and phospho-paxillin (Tyr118) antibodies failed to detect a significant change of phosphorylation state (Figure 2B). We also generated another phospho-specific antibody against p130Cas (P-Cas766Y: See Materials and Methods), and found consistent elevation in tyrosine phosphorylation of p130Cas by P-Cas766Y antibody in HSC44PE cells treated with 2 independent siRNAs for cortactin (Figure 2B). On the other hand, the level of phosphorylation of p130Cas was not significantly elevated in HSC57 cells (Figure

2B). There was no clear changes in the phosphorylation level of FAK or paxillin by the cortactin siRNAs in either HSC44PE cells or HSC57 cells (Figure 2B).

To confirm the role of hyperphosphorylated cortactin in these cells, we also generated MCF7 cell lines which have elevated tyrosine phosphorylation of cortactin. Original MCF7 cells showed high expression of cortactin with the minimum level of tyrosine phosphorylation (Figure 1A) and low expression of Fyn kinase (Figure 2C). A vector expressing the Flag-tagged Fyn kinase was introduced into MCF7 cells, and several clones with stable expression of Fyn kinase were isolated, and two of these clones were named as MCF-Fyn1 and MCF-Fyn2. The amount of Fyn protein in both cells was about 10-fold greater than that of endogenous Fyn kinase in original MCF7 cells (Figure 2C). Marked hyperphosphorylation of cortactin was observed in these two clones where Fyn kinase was introduced while original MCF7 cells or mock transfected cells (MCF-Vec) were not (Figure 2C). Knockout of cortactin greatly enhanced tyrosine phosphorylation of p130Cas both in MCF-Fyn1 cells and MCF-Fyn2 cells, but not in MCF7-Vec cells (Figure 2D and data not shown). These consistent results suggest that hyperphosphorylated cortactin may inhibit tyrosine phosphorylation of p130Cas in both HSC44PE and MCF-Fyn cells. Knockdown of cortactin also increased cell motility in both MCF-Fyn1 and MCF-Fyn2 cells while it blocked cell migration in parental MCF7 cells and MCF-Vec cells (Figure 1C, Figure 2E and data not shown). Similar results were obtained in the study using gastric cancer cells and it was demonstrated that hyperphosphorylation of cortactin switches the response of cell motility.

Since many reports have shown the significant role of phosphorylation of p130Cas in cell migration, we examined whether knockdown of p130Cas by siRNA impairs the cell motility of HSC44PE cells treated or non-treated with cortactin siRNA. Double treatment of Cas-siRNA and cort-siRNA completely impaired cell motility as well as treatment by Cas-siRNA alone, showing that p130Cas plays a dominant role in the regulation of cell motility of HSC44PE cells (Figure 3B). These results indicate the possibility that hyperphosphorylated cortactin may suppress cell migration through inhibiting tyrosine phosphorylation of p130Cas.

Recruitment of p130Cas to focal adhesion by treatment of cortactin siRNA

To further investigate the cause of tyrosine phosphorylation of p130Cas induced by knockdown of cortactin, we analyzed the subcellular localization of p130Cas, cortactin and focal adhesion proteins in HSC44PE cells. Total cortactin was widely expressed near the cell membrane in HSC44PE cells (Figures 4A and 4B) while phosphorylated cortactin detected by a phospho-specific antibody against cortactin Y421 is appeared at specific domain which seems to be as focal adhesion within the cell membrane (Figure 4B). It was further demonstrated that phosphotyrosine-containing cortactin was clearly colocalized with vinculin which is expressed at focal adhesion (Figure 4C). By the treatment with cortactin siRNA, both the signals detected

by total cortactin and cortactin Y421 were significantly weakened, suggesting these signals are cortactin-specific (Figure 4A).

In the control cells, p130Cas is mainly distributed in cytoplasm and only slightly expressed at focal adhesion (Figure 5B, upper panels). When cortactin is knocked down, a substantial amount of p130Cas comes to locate at focal adhesion (Figure 5B, lower panels), suggesting the loss of cortactin induced membrane localization of p130Cas. On the other hand, tyrosine phosphorylated p130Cas detected by phospho-specific antibody was specifically localized at the focal adhesion although the amount of tyrosine phosphorylation was greatly increased by the suppression of cortactin expression (Figure 5A). This observation may support the model that tyrosine phosphorylated cortactin expressed predominantly in focal adhesions interferes with the localization of p130Cas at the focal adhesion, which causes tyrosine phosphorylated p130Cas. Loss of hyperphosphorylated cortactin could therefore recruit p130Cas to the focal adhesion, which results in tyrosine phosphorylation of p130Cas, followed by enhancement of cell motility.

Discussion:

We explored the role of cortactin in cell motility by using RNAi technique in several gastric cancer cell lines that show various phosphorylation states of cortactin. It was revealed that knockdown of cortactin results in enhanced cell motility along with increased tyrosine phosphorylation of p130Cas in the cells that have hyperphosphorylated cortactin, whereas it impairs cell migration in the cells with a low level of tyrosine phosphorylated cortactin. In addition, knockdown of hyperphosphorylated cortactin caused recruitment of p130Cas to focal adhesion, which might result in enhanced cell migration. In this study, for the first time, we demonstrated that cortactin has a dual function in the regulation of cell motility, which depends upon its tyrosine phosphorylation state.

Amplification and overexpression of cortactin gene, *EMSI* have been identified in various cancers (2, 3, 6, 23). In our previous study, overexpression and elevated tyrosine phosphorylation of cortactin was selectively observed in the metastatic subgroup of murine melanoma cells with high migratory potential (16). Based on these results, we first hypothesized that the hyperphosphorylated cortactin may promote cell migration in cancer cells. In this study, gastric cancer cells that have hyperphosphorylated cortactin showed at least similar or higher migration potential compared with those cells with basal levels of tyrosine phosphorylation of cortactin (Figures 1A and C). However, unexpectedly, knockdown of cortactin in these cells further enhanced cell migration. The effect of cortactin knockdown was opposite in the cells with a low level of cortactin phosphorylation. This paradoxical outcome by cortactin knockdown was also confirmed in breast cancer cells MCF7, which expressed a significant

amount of cortactin although the level of tyrosine phosphorylation was quite low. Introduction of Fyn kinase to MCF7 cells significantly enhanced the tyrosine phosphorylation of cortactin. In this condition, loss of cortactin by siRNA enhanced cell migration while it had a negative effect on cell migration in the parental cells. Based on this finding, cortactin hyperphosphorylation may be induced as a negative feedback mechanism when cells acquire highly migratory potential.

Some of studies have shown that knockdown of cortactin results in impaired cell motility in hepatocellular carcinoma and head and neck squamous cell carcinoma cells (24, 25) while other studies have shown no significant effect on cell motility (8, 26), although all these studies lack information on the phosphorylation states of cortactin. Since it is suggested that cortactin differentially functions in cell migration depending on its phosphorylation state, the previous controversial results from the knockdown of cortactin should be revaluated from the viewpoint of its tyrosine phosphorylation state. A previous study shows positive effect of the cortactin phosphorylation on the cell migration by overexpression of normal cortactin and phosphorylation-defective mutants in the endothelial cells (27). Although this study does not mention about level of tyrosine phosphorylation of endogenous cortactin either, it might be weak in normal endothelial cells. Therefore positive effect of cortactin expression shown in the study might be consistent with our result using HSC57 or MCF7 cells, while dominant-negative effect of phosphorylation-defective mutant might indicate some different function of cortactin in the endothelial cells.

In our observation, knockdown of cortactin induced outstanding enhancement in tyrosine phosphorylation of p130Cas. Since there is no significant change in the phosphorylation of other substrates of SFKs such as FAK and paxillin, it is indicated that there exists some specific mechanism underlying the regulation of tyrosine phosphorylation state of p130Cas by cortactin. Unphosphorylated p130Cas is known to be mainly expressed in cytoplasm as shown in the Fig 5B, while localization of p130Cas in the focal adhesion is thought to be required for tyrosine phosphorylation of p130Cas (28, 29). The results of immunocytostaining indicate that tyrosine phosphorylated cortactin predominantly exists in the focal adhesion, and thus purging p130Cas from focal adhesion to lose the chance of being phosphorylated. Therefore, knockdown of cortactin might give chance for p130Cas to localize at the focal adhesion to be phosphorylated (Figure 5). p130Cas was originally found as a prominent substrate of SFKs including c-Src and Fyn during the transformation of cells (21, 30). It has been demonstrated that phosphorylated p130Cas in focal adhesion plays a regulatory role in cell spreading and cell migration (19,31-33), and knockdown of p130Cas actually abrogated cell migration in our gastric cancer cells HSC44PE even with the absence of cortactin (Figure 3A and B). These results indicate that activation of p130Cas-mediated signal might be

responsible for the enhancement of cell motility in the cells where hyperphosphorylated cortactin is knocked down.

Our study sheds new light on the crosstalk between cortactin and p130Cas, both of which are Src substrates. Such cross-regulation between SFKs substrates might give more optimized outcome out of overlapping or conflicting effects of SFKs signals. However, there is still a possibility that phosphorylated cortactin may also transduce specific signals regulating cell migration, which is independent of a function of p130Cas. As far as we examined, there was no significant effect on the morphology, cell-matrix adhesion or numbers of focal adhesions in HSC44PE cells by suppression of cortactin expression (Figure 5A and data not shown). On the other hand, it has been suggested that cortactin originally support the cell migration through several pathways and therefore its tyrosine phosphorylation may have an inhibitory effect on these pathways. Binding of cortactin with N-WASP via its SH3 domain may synergize in causing actin polymerization preceding cell migration, which is promoted by a serine kinase Erk and conversely inhibited by Src kinase (34). We illustrated all these signal pathways of phosphorylated cortactin in a schema (Figure 6). In summary, tyrosine phosphorylation of cortactin might act as a unique and naïve switch in the regulation of cell motility. Our study offers new insight into cortactin for understanding its biological function in cancer progression.

Materials and Methods

Cells culture

Human breast cancer cell line MCF7 was maintained in Dulbecco's modified Eagle's medium (DMEM) containing 10% (v/v) fetal bovine serum (FBS; GIBCOBRL, LIFE TECHNOLOGIES) and 50 ug/mL penicillin-streptomycin antibiotics. Human gastric cancer cell lines HSC57, HSC44As3, HSC44PE and HSC58As9 was supplied by Central Animal Laboratory, National Cancer Center Institute, Tokyo, Japan (Yanagihara *et al.*, 2004). They were maintained in RPMI 1640 supplemented with 10% fetal bovine serum and antibiotics.

Antibodies and Reagents

Anti-phosphotyrosine (4G10) and anti-cortactin (clone 4F11) antibodies were obtained from Upstate Biotechnology (Lake Placid, NY). Polyclonal antibodies Fyn3 and anti-FAK were purchased from Santa Cruz Biotechnology (Santa Cruz, CA). Anti-paxillin and anti-Green fluorescent protein (GFP) antibodies were purchased from Zymed (San Francisco, CA) and MBL (Nagoya, Japan) respectively. Anti-phospho-paxillin (Tyr118), anti-phospho-FAK (Tyr397) and anti-phospho-cortactin (Tyr421) antibodies were purchased from Cell Signaling Technology (Danvers, MA), Upstate Biotechnology (Lake Placid, NY) and Chemicon (Boronia Victoria, Australia) respectively. Anti-Flag-M2 antibody was obtained from SIGMA (Sigma, USA). Polyclonal antibodies against p130Cas (Cas2 & Cas3) and phospho-specific polyclonal

antibody P-Cas460Y were used as described previously (30, 35). Another phospho-specific antibody P-Cas766Y was generated by immunizing rabbits with a synthetic phospho-peptide, CMEDpYDpYVHL, which includes the phosphotyrosine-containing motifs in the Src-binding domain of p130Cas, after being conjugated with thymoglobulin. As secondary antibodies, horseradish peroxidase (HRP)-conjugated anti-rabbit and anti-mouse IgG (Amersham) were used. Polylysine, fibronectin (FN) and cycloheximide were purchased from SIGMA. Inhibitor of SFKs, 4-amino-5-(4-chlorophenyl)-7-(t-butyl) pyrazolo [3,4-d] pyrimidine (PP2) and the inactive structural analog 4-amino-7-phenylpyrazol [3,4-d] pyrimidine (PP3) were obtained from Calbiochem-Novabiochem Ltd.

RNAi experiments for cortactin and p130Cas

Two independent small interfering RNA (siRNA) of human cortactin, cort-siRNA1 and cort-siRNA2 for RNAi experiment were generated by Invitrogen Life Technologies. Cort-siRNA1 targets cortactin mRNA at 5'-CCCAGAAAGACUAUGUGAAAGGGUU-3' and Cort-siRNA2 targets at 5'-GGAGAAGCACGAGUCACAGAGAGAU-3'. The siRNA of human p130Cas was also generated by Invitrogen Life Technologies, using the target sequence 5'-CCAAGAUCUUUGUGGCGCACAGCAA-3'. For transient transfection of siRNA, the cells were plated at 1.5 X 10^5 per well on a six-well plate. Transfection of siRNAs was performed with Lipofectamine™ 2000 (Invitrogen Co.). After transfection for 72 hours, the cells were harvested for the biochemical analyses.

Infection of retroviral constructs

Retrovirus vector were used to express mouse cortactin fused with GFP (pjl6) and F421F466F482 triple mutant of mouse cortactin fused with GFP (pJL12)(4). Briefly, the retroviral vector and the packaging construct pCL-10A1 were cotransfected into 293T cells and culture fluid was harvested 72 hours post-transfection. HSC44PE cells were infected with the viral fluid in the presence of 4 mg/ml polybrene, and the infected cells were selected in the presence of 800 μg/ml Geneticin G418 (SIGMA) for a period of 2~3 weeks.

Establishment of stable MCF7 clones expressing Fyn kinase

Breast cancer cells MCF7 were grown in DMEM containing 10% FBS and antibiotics. On the night before transfection, the cells were seeded onto a 10-cm dish at a density of 9.0 X 10^5. Transfection of a vector expressing Fyn kinase with a tag of Flag (Fyn-Flag) and an original vector (pcDNA3.1) was performed according to the manufacture's instructions. Twenty-four hours after transfection, the cells were subjected to selection by Geneticin G418 (SIGMA) at a concentration of 800 μg/ml for a period of 2~3 weeks.

Immunoblotting and immunoprecipitation

For immunochemical analysis, cells were cultured in the incubator at 37℃ with 5% CO_2 for 48~72 hours, before the cells were lysed in 1% Triton X-100 buffer (50mM HEPES, 150mM NaCl, 10% glycerol, 1% Triton-X 100, 1.5mM $MgCl_2$, 1mM EGTA, 100mM NaF, 1mM Na_3VO_4, 10 μg/ml aprotinin, 10 μg/ml leupeptin, 1mM phenylmethylsulfony fluoride), and insoluble material was removed by centrifugation for 10 min. Protein concentration was analyzed by BCA Protein Assay (PIERCE) and the protein aliquots were separated by SDS-PAGE. Gels were transferred to the polyvinylidene difluoride membrane (Millipore) and subjected to immunoblotting. After blocking with 5% skim milk in TBST (100mM Tris-HCl pH 8.0, 150mM NaCl, 0.05% Tween 20) for 1h, blots were incubated with primary antibodies. In the case of 4G10, blocking was performed with Blocking One Solution (Nakarai Co.). Membranes were then washed three times with TBST, incubated with HRP-conjugated secondary antibodies for 30 min at RT, washed three times by TBST again and once by TBS (100mM Tris-HCl pH 8.0, 150mM NaCl), and visualized by autoradiography using a chemiluminescence reagent (Western Lighting, Perkin Elmer).

For immunoprecipitation, 500 μg of protein was mixed with 2 μg of antibodies and incubated for 1 hour on ice, and then samples were rotated with protein G-Sepharose beads (Amersham Pharmacia) for 2 hours at 4℃. The beads were washed three times with 1% Triton X-100 buffer and boiled in sample buffer (2% SDS, 0.1M Tris-HCl, pH6.8, 10% glycerol, 0.01% bromphenol blue, 0.1M dithiothreitol) for SDS-PAGE analysis.

Immunocytostaining

Around 5 ×10^4 cells were plated on 12-mm circle cover glasses on a 24-well plate, which were grown in DMEM with 10% FBS at 37℃ with 5% CO_2 for 24 hours. The 12-mm circle cover glasses were coated by fibronectin (FN) 10 μg/ml in PBS overnight before seeding the cells. Then cells were fixed in 4% paraformaldehyde in 0.1M sodium phosphate (pH 7.0) for 5 min, washed three times with PBS, and permeabilized with 0.1% Triton X-PBS for 10 min before blocking with 5% bovine serum albumin with TBST (0.15M NaCl, 1% Tris, pH 7.0, 0.05% Tween 20) for 10 min. Then the cells were incubated with the first antibody for 1 hour at room temperature. Cells were washed with PBS three times, and incubated with appropriate second Alexa antibodies (Molecular Probe) (1:500) in 5% goat serum with 3% BSA/TBST. All cover glasses were mounted in 1.25% DABCO, 50% PBS and 50% glycerol. The staining was visualized using a Radiance 2100 confocal microscopic system (Bio-Rad).

Cell migration assay

Migration assay was performed using modified Transwell chambers with polycarbonate Nucleopore membrane (FALCON™, BD, US). Precoated filters (6.5 mm in diameter, 8-μm pore size, FN 10 μg/ml) were rehydrated with 100 μl medium. Then, 4 x 10^4 cells in 100 μl serum-free DMEM supplemented were seeded onto the upper part of each chamber, whereas the lower compartments were filled with 600 μl of the same medium with 10% FBS. Following incubation for 8 hours at 37°C, non-migrated cells on the upper surface of

the filter were wiped out with a cotton swab, and the migrated cells on the lower surface of the filter were fixed and stained with Giemsa's Stain Solution (Azur-Eosin-Methylene Blue Solution, MUTO PURE CHEMICALS, Co. Japan). The total number of migrated cells was determined by counting cells in five microscopic fields per well at a magnification of 100X, and the extent of migration was expressed as the average number of the cells per microscopic field.

Acknowledgment

We thank Dr. Xi Zhan for mouse cortactin constructs and Dr. Hitoyasu Futami for critical reading of the manuscript. This study was supported by the Program for Promotion of Cancer Research (Japan) for the 3rd Term Comprehensive 10-Year-Strategy for Cancer Control.

References

1. Schuuring E, Verhoeven E, Litvinov S, Michalides RJ. The product of the EMS1 gene, amplified and overexpressed in human carcinoma, is homologous to a v-src substrate and is located in cell-substratum contact sites. *Mol Cell Biol* 1993; **13:** 2891-2898.
2. Campbell DH, deFazio A, Sutherland RL, Daly RJ. Expression and tyrosine phosphorylation of EMS1 in human breast cancer cell line. *Int J Cancer* 1996; **68:** 485-492.
3. Hui R, Ball JR, Macmillan RD, Kenny FS, Prall OW, Campbell DH *et al.* EMS1 gene expression in primary breast cancer relationship to cyclin D1 and oestrogen receptor expression and patient survival. *Oncogene* 1998; **17:** 1053-1059.
4. Li Y, Tondravi M, Liu J, Smith E, Haudenschild CC, Kaczmarek M *et al.* Cortactin potentates bone metastasis of breast cancer cells. *Cancer Res* 2001; **61:** 6906-6911.
5. Patel AM, Incognito LS, Schechter GL, Wasilenko WJ, Somers KD. Amplification and expression of EMS-1 (cortactin) in head and neck squamous cell carcinoma cell lines. *Oncogene* 1996; **12:** 31-35.
6. Freier K, Sticht C, Hofele C, Flechtenmacher C, Stange D, Puccio L *et al.* Recurrent coamplification of cytoskeleton-associated genes EMS1 and SHANK2 with CCND1 in oral squamous cell carcinoma. *Genes Chromosomes Cancer* 2006; **45:** 118-125.
7. Daly RJ. Cortactin signaling and dynamic actin networks. *Biochem J* 2004; **382:** 13-25.
8. Lua BL, Low BC. BPGAP1 interacts with cortactin and facilitates its translocation to cell periphery for enhanced cell migration. *Mol Biol Cell* 2004; **15:** 2873-2883.
9. Du Y, Weed SA, Xiong WC, Marshall TD, Parsons JT. Identification of a novel cortactin SH3 domain-binding protein and its localization to growth cones of cultured neurons. *Mol Cell Biol* 1998; **18:** 5838-5851.
10. Kowalski JR, Egile C, Gil S, Snapper SB, Li R, Thomas SM. Cortactin regulates cell migration through activation of N-WASP. *J Cell Sci* 2005; **118:** 79-87.
11. Wu H, Parsons JT. Cortactin, an 80/85-kilodalton pp60src substrate, is a filamentous actin-binding protein enriched in the cell cortex. *J Cell Biol* 1993; **120:** 1417-1426.
12. Kim L, Wong TW. Growth factor-dependent phosphorylation of the actin-binding protein cortactin is mediated by the cytoplasmic tyrosine kinase FER. *J Biol Chem* 1998; **273:** 23542-23548.

13. Gallet C, Rosa JP, Habib A, Lebret M, Levy-Toledano S Maclouf J. Tyrosine phosphorylation of cortactin associated with Syk accompanies thromoxane analogue-induced platelet shape change. *J Biol Chem* 1999; **274:** 23610-23616.
14. Campbell DH, Sutherland RL, Daly RJ. Signaling pathways and structural domains required for phosphorylation of EMS1/cortactin. *Cancer Res* 1999; **59:** 5376-5385.
15. Vidal, C. B. Geny, J. Melle, M. Jandrot-Perrus, M. Fontenay-Roupie. Cdc42/Rac1-dependent activation of the p21-activated kinase (PAK) regulates human platelet lamellipodia spreading implication of the cortical-actin binding protein cortactin. *Blood* 2002; **100:** 4462-4469.
16. Huang J, Asawa T, Takato T Sakai R. Cooperative roles of Fyn and cortactin in cell migration of metastatic murine melanoma. *J Biol Chem* 2003; **278:** 48367-48376.
17. Webb DJ, Parsons JT, Horwitz AF. Adhesion assembly, disassembly and turnover in migrating cells – over and over and over again. *Nat Cell Biol* 2002; **4:** 97-100.
18. Mitchison TJ, Cramer LP. Actin-base cell motility and cell locomotion. *Cell* 1996; **84:** 371-379.
19. Honda H, Oda H, Nakamoto T, Honda Z, Sakai R, Suzuki T *et al.* Cardiovascular anomaly, impaired actin bundling and resistance to Src-induced transformation in mice lacking p130Cas. *Nat Genet* 1998; **19:** 361-365.
20. Huang J, Hamasaki H, Nakamoto T, Honda H, Hirai H, Saito M *et al.* Differential regulation of cell migration, actin stress fiber organization, and cell transformation by functional domains of Crk-associated substrate. *J Biol Chem* 2002; **277:** 27265-27272.
21. Sakai R, Nakamoto T, Ozawa K, Aizawa S, Hirai H. Characterization of the kinase activity essential for tyrosine phosphorylation of p130Cas in fibroblasts. *Oncogene* 1997; **14:** 1419-1426.
22. Yanagihara K, Tanaka H, Takigahira M, Ino Y, Yamaguchi Y, Toge T *et al.* Establishment of two cell lines from human gastric scirrhous carcinoma that possess the potential to metastasize spontaneously in nude mice. *Cancer Sci* 2004; **95:** 575-582.
23. Zhang LH, Tian B, Diao LR, Xiong YY, Tian SF, Zhang BH *et al.* Dominant expression of 85-kDa form of cortactin in colorectal cancer. *J Cancer Res Clin Oncol* 2006; **132:** 113-120.
24. Chuma M, Sakamoto M, Yasuda J, Fujii G, Nakanishi K, Tsuchiya A *et al.* Overexpression of Cortactin is Involved in Motility and Metastasis of Hepatocellular Carcinoma. *J Hepatol* 2004; **41:** 629-636.
25. Rothschild BL, Shim AH, Ammer AG, Kelley LC, Irby KB, Head JA *et al.* Cortactin overexpression regulates actin-related protein 2/3 complex activity, motility, and invasion in carcinomas with chromosome 11q13 amplification. *Cancer Res* 2006; **66:** 8017-8025.
26. Barroso C, Rodenbusch SE, Welch MD, Drubin DG. A role for cortactin in Listeria monocytogenes invasion of NIH 3T3 cells, but not in its intracellular motility. *Cell Motil Cytoskeleton* 2006; **63:** 231-243.
27. Nakamoto T, Sakai R, Honda H, Ogawa S, Ueno H, Suzuki T *et al.* Requirements for localization of p130cas to focal adhesions. *Mol Cell Biol* 1997; **17:** 3884-3897.
28. Huang C, Liu J, Haudenschild CC, Zhan X. The role of tyrosine phosphorylation of cortactin in the locomotion of endothelial cells. *J. Biol Chem.* 1998; **273:** 25770-25776.
29. Sawada Y, Tamada M, Dubin-Thaler BJ, Cherniavskaya O, Sakai R, Tanaka S *et al.* Force sensing by mechanical extension of the Src family kinase substrate p130Cas. *Cell* 2006; **127:** 1015-1026.
30. Sakai R, Iwamatsu A, Hirano N, Ogawa S, Tanaka T, Mano H *et al.* A novel signaling molecule, p130, forms stable complexes in vivo with v-Crk and v-Src in a tyrosine phosphorylation-dependent manner.

EMBO J 1994; **13:** 3748-3756.

31. Klemke RL, Leng J, Molander R, Brooks PC, Vuori K, Cheresh DA. CAS/Crk coupling servers as a "molecular switch" for induction of cell migration. *J Cell Biol* 1998; **140:** 961-972.
32. Panetti TS. Tyrosine phosphorylation of paxillin, FAK and p130CAS: effects on cell spreading and migration. *Front Biosci* 2002; **7:** 143-150.
33. Pratt SJ, Epple H, Ward M, Feng Y, Braga VM, Longmore GD. The LIM protein Ajuba influences p130Cas localization and Rac1 activity during cell migration. *J Cell Biol* 2005; **168:** 813-824.
34. Martinez-Quiles N, Ho HY, Kirschner MW, Ramesh N, Geha RS. Erk/Src phosphorylation of cortactin acts as a switch on-switch off mechanism that controls its ability to activate N-WASP. *MolCell Biol* 2004; **24:** 5269-5280.
35. Miyake I, Hakomori Y, Misu Y, Nakadate H, Matsuura N, Sakamoto M *et al.* Domain-specific function of ShcC docking protein in neuroblastoma cells. *Oncogene* 2005; **24:** 3206-3215.

Titles and legends to figures

Figure 1. Changes in cell motility by knockdown of cortactin in gastric and breast cancer cells. (A) To evaluate expression and tyrosine phosphorylation of cortactin, cell lysates of gastric and breast cancer cell lines were immunoprecipitated with anti-cortactin antibody (2μg/mL), and immunoblotted by anti-phosphotyrosine antibody (4G10) and anti-cortactin antibody. The positions of cortactin isoforms (p85/80) are indicated by arrows. MCF7, HSC57 and HSC44As3 cells exhibited a low level of tyrosine phosphorylation of cortactin, whereas HSC44PE and HSC58As9 showed hyperphosphorylation of cortactin. Quantification of tyrosine phosphorylated cortactin was noted under the panel. The expression of total cortactin is shown in the bottom panel. **(B)** Amounts of cortactin in these cell lines at 72 hours after siRNA treatment are shown. **(C)** Cell motility in various cancer cell lines was evaluated by numbers of migrated cells on the membrane. Knockdown of cortactin by siRNA led inhibition of cell migration in HSC57, HSC44As3 and MCF7 cells with hypophosphorylated cortactin, whereas it resulted in increase of cell migration in HSC44PE and HSC58As9 cells with hyperphosphorylated cortactin. **(D)** HSC44PE cells (Parent) and HSC44PE cells stably expressed mouse cortactin (mcort-WT) or F421F466F482 triple mutant of mouse cortactin (mcort-Mut) fused with GFP were treated with or without cortactin siRNA. Cells were lysed 72 hours after treatment and immunoblotted for cortactin and GFP. The concentration of total proteins was confirmed by the same membrane rehybridized with anti-α-tubulin antibody. Cortactin siRNA downregulates endogenous human cortactin (endo) but not exogenous mouse cortactins (exo). Tyrosine phosphorylation of mouse cortactins was analyzed by immunoprecipitation of total cortactin and immunoblotting with anti-phosphotyrosine antibody (4G10). The quantification of immunoprecipitated cortactin is shown in the bottom (IB: cortactin). **(E)** Effect of the rescue of mouse cortactin expression on cell migration in cortactin knockdown HSC44PE cells were analyzed as described. Rescue of tyrosine phosphorylated cortactin (mcort-WT) affected the inhibition of cells migration but non-tyrosine phosphorylated cortactin (mcort-Mut) did not.

Figure 2. Analysis of cell motility in MCF clones with hyperphosphorylated cortactin. (A) HSC57 and HSC44PE cells were treated with cortactin siRNA for 72 hours, the whole cell lysates were subjected to immunoblotting assay by antibody 4G10 to see phosphotyorsine-containing proteins. The phosphotyrosine-containing protein around 120~130KDa was significantly enhanced as indicated by a square bracket. **(B)** Marked elevation of phosphorylation of p130Cas at tyrosine 460 and tyrosine 766 in HSC44PE cells was confirmed by specific anti-phospho-Cas antibodies (P-Cas460Y and P-Cas766Y) using two independent cortactin siRNAs. Immunoblotting by anti-cortactin, anti-Cas2, anti-phospho-FAK (Tyr397), anti-phospho-paxillin (Tyr118) and anti-tubulin antibodies are also shown. **(C)** Stable

clones of MCF7 cells expressing Flag-tagged Fyn kinase (MCF-Fyn1 and MCF-Fyn2) or vector alone (MCF-Vec) were established (see Materials and Methods). Left panels show immunoblotting by anti-Flag, anti-Fyn3 and anti-tubulin antibodies to demonstrate high expression of Flag-Fyn in these clones. Right panels indicate that the tyrosine phosphorylation of cortactin was markedly induced in MCF-Fyn1 and MCF-Fyn2 clones with no significant change in total cortactin expression. **(D)** Enhancement of phosphorylation of p130Cas at tyrosine 460 and tyrosine 766 in MCF-Fyn1 cells treated with two independent cortactin siRNAs was confirmed by specific anti-phospho-Cas antibodies (P-Cas460Y and P-Cas766Y). **(E)** Effect of cortactin siRNA on cell migration of MCF7-Fyn clones was analyzed as described.

Figure 3. Knockdown of p130Cas blocks cell migration of HSC44PE cells regardless to the expression of cortactin. (A & B) HSC44PE cells were treated with either cortactin siRNA or p130Cas siRNA alone, or both and cell migration was analyzed as described. (A) Expression of cortactin, p130Cas (Cas2) and phosphorylated p130Cas (pCas460Y) was analyzed to check the effect of each siRNA.(B) By treatment with siRNA of Cas, cell migration of HSC44PE cells was totally inhibited regardless of the amount of cortactin expression.

Figure 4. Localization of cortactin and tyrosine phosphorylated cortactin in HSC44PE cells. (A) HSC44PE cells were transfected with cortactin siRNA or control siRNA for 72 hours followed by immunocytostaining with anti-cortactin (green) and anti-phospho-cortactin (Tyr421: red) antibody. **(B)** HSC44PE cells were immunostaied with anti-phospho-cortactin (Tyr421: red) and anti-cortactin (green) antibodies. **(C)** HSC44PE cells were immunostained with anti-phospho-cortactin (Tyr421: red) and anti-vinculin (green) antibodies. Merged image (Merge) indicates that of tyrosine phosphorylated cortactin localizes at focal adhesions which are stained by anti-vinculin.

Figure 5. Changes in localization of p130Cas by treatment with cortactin siRNA. (A) HSC44PE cells were transfected with cortactin siRNA or control siRNA for 72 hours, before localization of phosphorylated p130Cas was analyzed by immunocytostaining with P-Cas766Y antibody. Anti-vinculin antibody was used to visualize focal adhesions. Merged images indicate that tyrosine phosphorylated p130Cas which was greatly increased by cortactin siRNA specifically localizes at focal adhesion. **(B)** In HSC44PE cells treated with control or cortactin siRNA, localization of p130Cas was analyzed by anti-Cas3 antibody. Potion of p130Cas shows distinct colocalization with vinculin at focal adhesion in cells treated with cortactin siRNA, while staining of vinculin and p130Cas did not significantly overlapped in cells treated with control siRNA.

Figure 6. Schematic view of multiple roles of cortactin in the regulation of cancer cell motility.

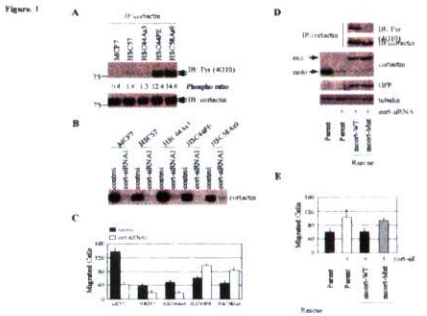

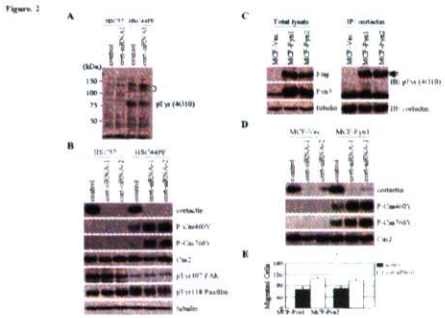

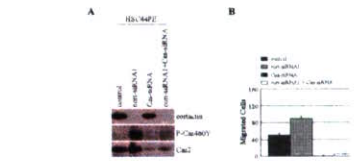

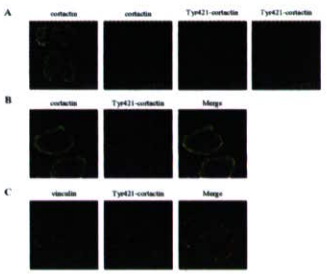

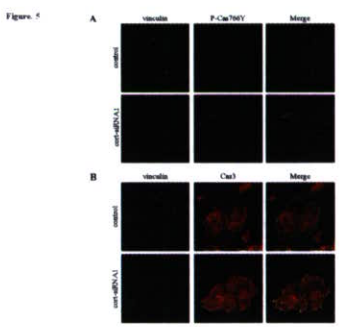

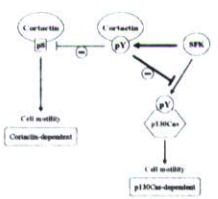

Supplementary Figure

Involvement of SFKs in gastric cancer cells HSC44PE. **(A)** Src family inhibitor PP2 impaired tyrosine phosphorylation of cortactin in HSC44PE gastric cancer cells. HSC44PE cells were treated with 10μM PP2 or PP3 for 3 hours prior to cell lyses. The whole-cell lysates were immunoprecipitated by anti-cortactin antibody, and immunoblotted by anti-phosphotyrosine antibody 4G10. **(B)** Expression of three major Src family members (Src, Fyn and Yes) in HSC57 and HSC44PE cells. Total 20 μg cell lysates were subjected to immunoblotting analysis by anti-Src, anti-Fyn3 and anti-Yes antibodies. (C) Lysates of HSC44PE cells were immunoprecipitated by anti-Fyn3 antibody or rabbit Ig-G (negative control), and subjected to immunoblotting by anti-cortactin antibody. The position of cortactin protein is indicated by the arrow.

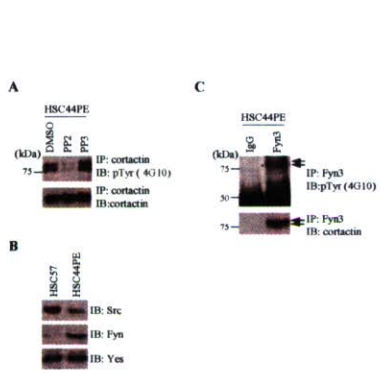

THE JOURNAL OF BIOLOGICAL CHEMISTRY
Vol. 280, No. 12, Issue of March 25, pp. 11467–11474, 2005
Printed in U.S.A.

The Fission Yeast Protein Ker1p Is an Ortholog of RNA Polymerase I Subunit A14 in *Saccharomyces cerevisiae* and Is Required for Stable Association of Rrn3p and RPA21 in RNA Polymerase I*

Received for publication, September 29, 2004, and in revised form, January 10, 2005
Published, JBC Papers in Press, January 12, 2005, DOI 10.1074/jbc.M411150200

Yukiko Imazawa‡§¶, Koji Hisatake‡, Hiroshi Mitsuzawa‖, Masahito Matsumoto‡, Tohru Tsukui‡¶, Kaori Nakagawa‡§, Tomoyoshi Nakadai‡, Miho Shimada‡, Akira Ishihama, and Yasuhisa Nogi‡ ‡‡**

*From the ‡Department of Molecular Biology, Saitama Medical School, 38 Morohongo, Moroyama, Iruma-gun, Saitama 350-0495, Japan, the §Japan Science and Technology Corporation Center, Kawaguchi, Saitama 332-0012, Japan, the ¶Research Center for Genomic Medicine, Saitama Medical School, Hidaka, Saitama 350-1241, Japan, the ‖Department of Molecular Genetics, National Institute of Genetics, Mishima, Shizuoka 411-8540, Japan, and the **Nippon Institute for Biological Science, Oume, Tokyo 198-0024, Japan*

A heterodimer formed by the A14 and A43 subunits of RNA polymerase (pol) I in *Saccharomyces cerevisiae* is proposed to correspond to the Rpb4/Rpb7 and C17/C25 heterodimers in pol II and pol III, respectively, and to play a role(s) in the recruitment of pol I to the promoter. However, the question of whether the A14/A43 heterodimer is conserved in eukaryotes other than *S. cerevisiae* remains unanswered, although both Rpb4/Rpb7 and C17/C25 are conserved from yeast to human. To address this question, we have isolated a *Schizosaccharomyces pombe* gene named *ker1*$^+$ using a yeast two-hybrid system, including *rpa21*$^+$, which encodes an ortholog of A43, as bait. Although no homolog of A14 has previously been found in the *S. pombe* genome, functional characterization of Ker1p and alignment of Ker1p and A14 showed that Ker1p is an ortholog of A14. Disruption of *ker1*$^+$ resulted in temperature-sensitive growth, and the temperature-sensitive deficit of *ker1*Δ was suppressed by overexpression of either *rpa21*$^+$ or *rrn3*$^+$, which encodes the rDNA transcription factor Rrn3p, suggesting that Ker1p is involved in stabilizing the association of RPA21 and Rrn3p in pol I. We also found that Ker1p dissociated from pol I in post-log-phase cells, suggesting that Ker1p is involved in growth-dependent regulation of rDNA transcription.

There are three distinct types of eukaryotic nuclear RNA polymerases: RNA polymerase (pol)[1] I, pol II, and pol III. Among eukaryotic organisms, the structure and function of RNA polymerases in *Saccharomyces cerevisiae* have been studied fairly extensively (1–4). *S. cerevisiae* pol I consists of 14 subunits. The core structure contains 10 subunits (A190, A135, AC40, AC19, Rpb5, Rpb6, Rpb8, Rpb10, Rpb12, and A12.2) and is believed to be sufficient for nonspecific transcription, but not for accurate initiation of transcription (5). In fact, pol I requires four specific subunits (A49, A43, A34.5, and A14) for specific transcription of rDNA. A43 is also essential for cell growth (6), whereas A49 (7), A34.5 (8), and A14 (9) are dispensable.

Much attention has recently been focused on the A14 and A43 subunits in view of the structural and functional conservation of these two subunits in eukaryotes. A43 is conserved in a variety of eukaryotes (10) and shows amino acid sequence similarity to Rpb7 (a specific subunit of pol II), C25 (a specific subunit of pol III), and RpoE (a subunit of archaeal RNA polymerases) across multiple RNA polymerases (11). Furthermore, A43 forms a heterodimer with A14 that is similar to the Rpb4/Rpb7 (11, 12), C17/C25 (13), and RpoF/RpoE (14) heterodimers in pol II, pol III, and archaeal RNA polymerases, respectively. It should be noted that Rpb4, C17, and RpoF have mutual sequence similarity and are grouped into a gene family, but no obvious homolog of A14 has been found in available data bases. A14 and Rpb4 are required for the stable assembly of A43 and Rpb7, respectively, in their respective RNA polymerases, suggesting a functional similarity of A14 to Rpb4 (5, 11, 15, 16). The position of A14/A43 in the three-dimensional structure of pol I has been deduced to be similar to that of Rpb4/Rpb7, forming an upstream interface with the C-terminal domain of Rpb1 to interact with transcription factor IIB for pol II recruitment to the pol II promoter (4) and, furthermore, playing a role in the processing of the nascent RNA transcript (17). Consistent with the proposed position in pol I, A14/A43 also interacts with an rDNA-specific transcription factor (Rrn3p) for pol I recruitment to the rDNA promoter (10) and is able to bind to single-stranded RNA (18). Interestingly, C17/C25 in pol III is also reported to interact with transcription factor IIIB, which recruits pol III to the pol III promoter (19).

The mechanism of the down-regulation of rDNA transcription (20–24) is now believed to be as follows. Only a small fraction of pol I associated with Rrn3p is able to recognize the components of the preinitiation complex, resulting in pol I recruitment to the rDNA promoter (25–28). A43 in pol I is responsible for associating with Rrn3p (10), and the association of A43 with Rrn3p is inhibited in post-log-phase cells (including nutrient-starved or growth-arrested cells) (24, 26), resulting in a drastic decrease in pol I recruitment to the promoter (29).

* This work was supported by the Core Research for Evolutional Science and Technology of the Japan Science and Technology Corporation, by a Human Frontier Science Program Organization grant, and by a grant for the promotion of the advancement of education and research in graduate schools from the Ministry of Education, Culture, Sports, Science, and Technology of Japan. The costs of publication of this article were defrayed in part by the payment of page charges. This article must therefore be hereby marked "*advertisement*" in accordance with 18 U.S.C. Section 1734 solely to indicate this fact.

The nucleotide sequence(s) reported in this paper has been submitted to the DDBJ/GenBank™/EBI Data Bank with accession number(s) AB07137.

‡‡ To whom correspondence should be addressed. Tel.: 81-492-76-1490; Fax: 81-492-94-9751; E-mail: yasunogi@saitama-med.ac.jp.

[1] The abbreviations used are: pol, RNA polymerase; 3-AT, 3-amino-1,2,4-triazole; HA, hemagglutinin; Gal4DB, Gal4 DNA-binding domain; CMV, cytomegalovirus; GFP, green fluorescent protein; DAPI, 4′,6-diamidino-2-phenylindole.

TABLE I
Yeast strains and plasmids

Strains and plasmids	Description
Strains	
S. pombe	
JY742	*h⁺ ade6-M216 ura4-D18 leu1*
JY745	*hj⁻ ade6-M210 ura4-D18 leu1*
IZ2	Derivative of JY742 expressing RPA140 tagged with His_6-FLAG (42)
YI28	Derivative of IZ2 expressing *ker1⁺*-HA_3
YI29	Diploid (crossing JY742 with JY745) carrying *ker1Δ::ura4⁺/ker1⁺*
YI30	*h⁻ ker1Δ::ura4⁺ ade6 ura4-D18 leu1*
S. cerevisiae	
Y190	*MATa ade2-101 ura3-52 his3-Δ200 lys2-801 trp1-901 leu2-3,112 gal4Δ gal80Δ LYS2::GAL1-HIS3 URA3::GAL1-lacZ*
Plasmids	
pKI45	Derivative of KS(+) cloned with full-length cDNA of *rpa21⁺* between XhoI and EcoRI sites
pYI77	Derivative of pAS2-1 expressing Gal4DB-RPA21, *TRP1*, 2μm
pKS406	Derivative of pSGA (47) expressing GFP fusion proteins under control of *nmt1* promoter, *ars1*, *LEU2*
pYI193	Derivative of pKS406 expressing GFP-Ker1p
pYI200	Derivative of pKS406 expressing GFP-fibrillarin
pYN1235	Derivative of pGEM3ZpBR322ura4⁺pBR322 with BamHI site introduced into HindIII site (55)
pYN1237	Derivative of KS(+); HA_3-TAG sequence (triple-HA epitope tagged with TAG) inserted between SmaI and SpeI sites; 2.5-kb BamHI-BamHI *ura4⁺* fragment excised from pYN1235 inserted at BglII site created downstream of HA_3-TAG sequence
pAUR224	Expression vector under control of CMV promoter, *aur1ʳ*, *ars1*
pYI195	Derivative of pAUR224 expressing full-length Ker1p under control of CMV promoter
pYI176	Derivative of pYN1237 carrying 1.0-kb fragment of 5′-flanking and coding sequence of Ker1p-HA_3, *ura4⁺*, and 1.0-kb fragment of 3′-flanking sequence of *ker1⁺*
pGK100	Derivative of pDB248 carrying *nuc1⁺/rpa190⁺* (37)
pYI185	Derivative of KS(+) carrying 0.88-kb fragment of 5′-flanking region of *ker1⁺* between XhoI and BamHI sites and 1.0-kb fragment of 3′-flanking region of *ker1⁺* between NotI and SacI sites
pYI186	Derivative of pYI185 with *ura4⁺* inserted at BamHI site
pREP41	Expression vector under control of modified *nmt1* promoter, *LEU2*, *ars1* (56)
pREP81	Expression vector under control of modified *nmt1* promoter, *LEU2*, *ars1* (56)
pYI40	Derivative of pREP81 with NdeI site converted to BglII site (41)
pYI82	Derivative of pYI40 expressing *rpa21⁺* cDNA under control of weak *nmt1* promoter (41)
pKI27	Derivative of pREP81 expressing full-length *rrn3⁺* under control of *nmt1* promoter
pYI210	Derivative of pYI40 expressing full-length *ker1⁺* under control of *nmt1* promoter

Thus, the molecular function of A43 and Rrn3p deserves further study to resolve long-standing questions regarding growth-dependent transcription of rDNA (30).

It is firmly established that all 12 and all 17 subunits of *S. cerevisiae* pol II and pol III, respectively, are conserved in human pol II and pol III (31, 32). However, it is not clear whether all 14 subunits identified in *S. cerevisiae* pol I are conserved in other eukaryotes (33, 34). To gain further insight into the structure and function of pol I, we have been studying pol I of *Schizosaccharomyces pombe*, which is only distantly related to *S. cerevisiae*, but is amenable to genetic analysis (35). To date, it is known that *S. pombe* pol I consists of at least 12 subunits. The two largest, RPA190 and RPA140, are homologous to A190 and A135, respectively (36, 37). The two smaller subunits, RPA42 and RPA17, correspond to AC40 and AC19, respectively (38, 39). Five common subunits (Rpb5, Rpb6, Rpb8, Rpb10, and Rpb12) are shared by pol II and pol III (12), and SpRPA12 is a functional homolog of A12.2 (40). Thus, the 10-subunit core structure of pol I has been well conserved between the two yeasts through evolution. Moreover, the two specific subunits in *S. pombe*, RPA21 and RPA51, have been identified to be related to A43 and as a functional homolog of A49, respectively, suggesting that the pol I architecture in *S. pombe* is likely to be analogous to that in *S. cerevisiae* (41, 42).

In this study, we demonstrate that a newly isolated protein, Ker1p, is an ortholog of A14 and that the Ker1p/RPA21 heterodimer in *S. pombe* is the functional counterpart of A14/A43 in *S. cerevisiae*. We also show novel aspects of Ker1p that have not been previously observed in A14 and suggest that Ker1p is involved in growth-dependent transcription of rDNA.

EXPERIMENTAL PROCEDURES

Media, Strains, and Genetic Techniques—The yeast plasmids and strains used are listed in Table I. Minimal medium with or without thiamine and supplemented with appropriate amino acids and yeast extract/dextrose medium were prepared to grow *S. pombe* cells as described previously (35). Yeast extract/peptone/dextrose medium and synthetic dextrose medium were prepared as described previously (43). Synthetic dextrose medium lacking tryptophan and leucine and synthetic dextrose medium containing 25 mM 3-amino-1,2,4-triazole (3-AT) were used. Minimal medium containing 0.1–0.4 μg/ml aureobasidin A was also used. Disruption of chromosomal *ker1⁺* was carried out as follows. Diploid cells (a cross between JY742 and JY745 cells) were transformed with the 4.5-kb XhoI-SacI linear fragment containing *ker1Δ::ura4⁺* from pYI186. To replace Ker1p with Ker1p-HA_3, a 5.0-kb XhoI-SacI fragment from pYI176 (see below) was transformed into strain IZ2, resulting in YI28.

Plasmids—For two-hybrid screening, Gal4DB-*rpa21⁺* (pYI77) was constructed as follows. 0.52-kb *rpa21⁺* cDNA was amplified by PCR using pKI45 containing a full-length 0.52-kb cDNA of *rpa21⁺* (41) as a template and cloned between the SmaI and XhoI sites of pAS2-1 (44) to fuse Gal4DB to RPA21 in-frame. To construct deletion derivatives of *rpa21⁺*, pKI45 was also used as template DNA for PCR amplification. pYI106 expresses RPA21 with the N-terminal 56 amino acids truncated fused to Gal4DB, whereas pYI105 expresses RPA21 with the C-terminal 60 amino acids truncated fused to Gal4DB. To replace chromosomal *ker1⁺* with *ker1⁺*-HA_3, a PCR-amplified 1317-bp XhoI-SmaI fragment of the 5′-untranslated region and open reading frame of *ker1⁺* and a 1017-bp NotI-SacI fragment of the 3′-flanking region of *ker1⁺* were cloned successively between the XhoI and SmaI sites and the NotI and SacI sites of pYN1237, generating pYI176. To express Ker1p under the control of the cytomegalovirus (CMV) promoter in *S. pombe*, full-length *ker1⁺* (441 bp) was amplified from JY742 DNA by PCR and cloned between the XhoI and BamHI sites of pAUR222 (TaKaRa), resulting in pYI195. To study the cellular localization of Ker1p, full-length *ker1⁺* was amplified from JY742 DNA, and the 441-bp fragment was cloned between the NotI and BamHI sites of pKS406 to express a GFP-Ker1p fusion protein, resulting in pYI193. A GFP-fibrillarin fusion construct was made using a 912-bp fragment of the *fib* gene encoding fibrillarin, which was amplified by PCR from JY742 DNA and cloned between the NotI and BamHI sites of pKS406, resulting in pYI200. To construct a disrupted *ker1Δ::ura4⁺* allele, we amplified the 880-bp 5′-untranslated sequence of *ker1⁺* flanked by the XhoI and BamHI sites and the 1.0-kb 3′-untranslated sequence of *ker1⁺* flanked by the NotI and SacI sites from the JY742 genome. Each PCR product was cloned successively between the XhoI and BamHI sites and between the NotI and SacI sites of pBluescript II KS(+), resulting in pYI185. Then, the 2.5-kb BamHI-BamHI DNA fragment of *ura4⁺* obtained from pYN1235 was cloned into the BamHI site of the resulting plasmid, generating pYI186. To construct pKI27, full-length *rrn3⁺* was amplified by PCR from JY742 DNA and cloned between the SalI and SmaI sites of pREP81. To express *ker1⁺* under the control of the *nmt1* promoter, full-length *ker1⁺* was amplified by PCR from JY742 DNA and cloned between the SalI and BamHI sites of pYI40, generating pYI210. *Pfu* DNA polymerase was used for PCR, and DNA sequencing analysis was used to confirm the PCR product.

Two-hybrid Screening—pYI77 expressing a Gal4DB-RPA21 bait was transformed into the reporter strain Y190. Y190 carrying pYI77 was transformed with an *S. pombe* cDNA library fused to Gal4 activation domain in pGAD-GH (Clontech). The 3-AT-resistant and His^+ transformants were screened on synthetic dextrose medium plates without Trp and Leu and containing 25 mM 3-AT. *lacZ* activation was examined by a filter lifting assay (38).

Fluorescence Microscopy of GFP Fusion Proteins—To visualize the nuclear chromatin region, cells were stained with 4′,6-diamidino-2-phenylindole (DAPI) at 1 mg/ml. Fluorescent images were obtained with a Fujix HC-2500 CCD camera using a Zeiss Axioskop fluorescence microscope.

Immunoprecipitation—*S. pombe* cells were grown in yeast extract/dextrose medium and harvested in mid-log phase. Preparation of cell extracts and immunoprecipitation with anti-HA epitope monoclonal antibody 12CA5 (Roche Applied Science) and anti-RPA190 antibody were carried out as described by Mitsuzawa *et al.* (45). Immunoblotting was performed essentially as described previously (39) using polyclonal antibodies against RPA190, RPA140, RPA21, and Rpb1 (pol II) (41, 46).

Biochemical Fractionation of pol I—pol I was partially purified as described previously (46). Whole cell extract from strain YI28 was loaded onto a nickel-nitrilotriacetic acid-agarose column. The proteins eluted with 200 mM imidazole were loaded onto a DEAE-Sephadex A25 column and eluted with a 50–620 mM ammonium sulfate gradient. Fractions were examined by SDS-PAGE, followed by Western blotting using antibodies against RPA190, RPA21, and HA. (Ker1p was tagged with HA_3 in strain YI28.)

Phosphatase Treatment—Whole cell extract was prepared form strain YI28, and 1.6 mg of protein was immunoprecipitated with anti-RPA190 antibody (10 μl of antiserum) as described above. The precipitates were washed three times with 20 mM HEPES-KOH (pH 7.6), 150 mM potassium acetate, 20% glycerol, 0.1% Nonidet P-40, and 1 mM dithiothreitol and once with HM buffer (50 mM HEPES-KOH (pH 7.6) and 1 mM $MgCl_2$). The pellet was resuspended in 1 ml of HM buffer, divided into four aliquots, centrifuged again, resuspended with 100 μl of HM buffer, and incubated for 10 min at 30 °C. Calf intestine alkaline phosphatase (30 units, 1.5 μl; Roche Applied Science) was added to one tube and incubated for 20 min at 30 °C. The reaction was stopped by addition of SDS sample buffer and heating at 95 °C for 5 min. In controls, sodium pyrophosphate (final concentration of 5.4 mM) was added with or without alkaline phosphatase, and the sample was then treated as described above. No treatment was performed for the fourth sample. All samples were subjected to 8% SDS-PAGE, followed by immunoblot analysis with anti-HA antibody.

RESULTS

Identification of a Novel Protein (Ker1p) That Interacts with the RPA21 Subunit—To identify protein(s) that interact with RPA21, we generated a Gal4DB-RPA21 fusion construct in pAS2-1 (pYI77) and introduced it into the *S. cerevisiae* two-hybrid reporter strain Y190. Subsequently, we introduced an *S. pombe* cDNA library fused to the Gal4 activation domain into the Y190 strain carrying pYI77. We selected ~10^7 Leu^+ transformants and screened colonies showing 3-AT resistance and a *lacZ*-positive phenotype. In total, 27 transformants showing 3-AT resistance and the *lacZ*-positive phenotype were obtained, and the responsible plasmids carrying cDNA fused to the Gal4 activation domain were retrieved (data not shown). Nucleotide sequencing of the retrieved plasmids indicated that all of the cDNAs encoding the protein shown to interact with RPA21 were derived from the same gene; one group lacked the C-terminal 30 amino acids, and another retained the full-length gene, indicating that the C-terminal 30 amino acids are not required for interaction with RPA21 in the yeast two-hybrid method. The gene isolated by the two-hybrid system encodes a protein of 147 amino acids with a calculated molecular mass of 16,976 Da and a calculated pI of 6.25. The predicted protein is very hydrophilic and contains many charged amino acids: 21 lysine residues, 9 arginine residues, 24 glutamic acid residues, and 7 aspartic acid residues (see Fig. 7). Therefore, we have named this protein Ker1p (for lysine (K) and glutamic acid (E)-rich protein 1) and the gene encoding it *ker1⁺*. No proteins homologous to Ker1p were observed in an initial data base search.

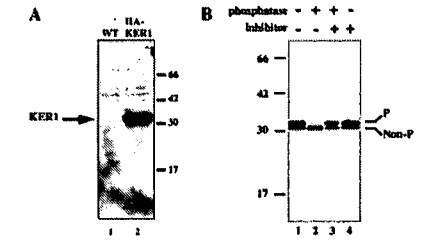

FIG. 1. **Ker1p can be phosphorylated.** *A*, apparent molecular mass of Ker1p. Extracts prepared from *S. pombe* cells of strains IZ2 (wild type (*WT*)) and YI28 expressing Ker1p-HA_3 (*HA-KER1*) were subjected to SDS-PAGE, followed by immunoblot analysis with monoclonal antibody 12CA5. In *lanes 1* and 2, 40 μg of crude extract was loaded. *B*, Ker1p is a phosphorylated protein. Ker1p-HA_3 was immunoprecipitated from a whole cell extract of strain YI28 with monoclonal antibody 12CA5. The immunoprecipitates were treated as follows: no treatment (*lane 1*), alkaline phosphatase (*lane 2*), alkaline phosphatase and a phosphatase inhibitor (sodium pyrophosphate; *lane 3*), and the inhibitor alone (sodium pyrophosphate; *lane 4*). After treatment, samples were subjected to SDS-PAGE, followed by immunoblot analysis with monoclonal antibody 12CA5. Molecular mass standards (in kilodaltons) are indicated on the right in *A* and on the *left* in *B*. *P*, phosphorylated Ker1p; *Non-P*, non-phosphorylated Ker1p.

Apparent Molecular Mass of Ker1p-HA_3—To determine the apparent molecular mass of Ker1p, a YI28 strain expressing Ker1p-HA_3 was constructed. Whole cell extracts prepared from YI28 and the parental strain IZ2, in which Ker1p had not been tagged, were subjected to SDS-PAGE, followed by immunoblotting with anti-HA monoclonal antibody 12CA5. Fig. 1*A* shows that Ker1p-HA_3 was detected as a doublet of bands at 30 and 32 kDa, including a triple-HA sequence (4.3 kDa). Since the calculated molecular mass of Ker1p is ~17 kDa, it appears that Ker1p-HA_3 migrates abnormally on SDS-polyacrylamide gel, for unknown reasons.

Ker1p Is Phosphorylated—The predicted amino acid sequence of Ker1p suggested that it contains many consensus phosphorylation sites for protein kinase A (Ser^{14}), protein kinase C (Ser^{14}, Ser^{22}, and Ser^{94}), casein kinase I (Ser^{45}), casein kinase II (Ser^{41} and Thr^{89}), and glycogen synthase kinase I (Ser^{41}, Ser^{45}, Ser^{94}, and Thr^{89}) (see Fig. 7). We considered the possibility that Ker1p is phosphorylated and that both phosphorylated and non-phosphorylated forms were detected as doublet bands by immunoblotting in Fig. 1*A*. Therefore, Ker1p-HA_3 was first immunoprecipitated with anti-HA antibody, and the immunoprecipitates were then treated with alkaline phosphatase in the absence or presence of a phosphatase inhibitor. As shown in Fig. 1*B*, phosphatase treatment resulted in the appearance of only the faster moving 30-kDa band (*lane 2*). No treatment (*lane 1*), treatment with phosphatase and an inhibitor (*lane 3*), or treatment with the inhibitor only (*lane 4*) generated two bands of 30 and 32 kDa, similar to those observed in Fig. 1*A* (*lane 2*). Therefore, we conclude that the 30-kDa band represents non-phosphorylated Ker1p-HA_3 and that the 32-kDa band represents phosphorylated Ker1p-HA_3.

Ker1p Is Localized Predominantly in the Nucleolus—Because Ker1p interacts with RPA21 of pol I, which localizes specifically in the nucleolus, we examined whether Ker1p also localizes in the nucleolus using a GFP-Ker1p fusion protein. Fig. 2 (*A–C*) shows that GFP-Ker1p formed a dense, crescent-shaped structure that occupied one side of the nucleus and that the crescent-shaped region was not stained well by DAPI. The observed crescent-shaped structure with much reduced DNA staining is the most obvious characteristic of the yeast nucleolus (37, 47, 48). However, GFP-Ker1p was also observed in the DAPI-stained region (Fig. 2*B*), and it might be possible that GFP-Ker1p also localizes outside the nucleolus due to overproduction under the control of the strong *nmt1* promoter. For controls, we examined localization of GFP itself and observed a clear cytoplasmic distribution (Fig. 2, *D–F*). We also examined the localization of the nucleolar protein fibrillarin (GFP-fibrillarin) expressed in the same GFP fusion vector and found that it localized specifically in the crescent-shaped nucleolus (Fig. 2, *G–I*). As expected, the crescent-shaped region in the nucleus shows much lower DAPI staining in Fig. 2*G*. Taken together, we conclude from these results that Ker1p is predominantly localized in the nucleolus, although it is also possible that a certain fraction of Ker1p localizes in the nucleoplasm.

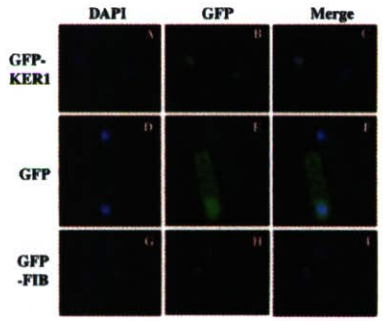

FIG. 2. **Ker1p predominantly localizes in the nucleolus.** The GFP-Ker1p (*GFP-KER1*; *A–C*) or GFP-fibrillarin (*GFP-FIB*; *G–I*) fusion protein or GFP alone (*D–F*) was expressed in *S. pombe* strain JY742. DNA was visualized by DAPI staining in *A*, *D*, and *G*. The localization of GFP fusion proteins and GFP is shown in *B*, *E*, and *H*. Merged images are shown in *C*, *F*, and *I*.

Co-immunoprecipitation of Ker1p and pol I—The apparent nucleolar localization of Ker1p prompted us to study the physical interaction of RPA21 (pol I) and Ker1p *in vivo*. Therefore, extracts prepared from cells expressing Ker1p-HA_3 were immunoprecipitated with anti-HA antibody (12CA5) beads, and coprecipitated proteins were detected by immunoblotting. Fig. 3*A* shows that pol I subunits RPA190, RPA140, and RPA21 co-immunoprecipitated with Ker1p, suggesting that Ker1p associates with pol I *in vivo*. The association is specific for pol I because the pol II subunit Rpb1 was not co-immunoprecipitated (Fig. 3*A*, *fourth panel*). Conversely, Ker1p co-immunoprecipitated with RPA140 and RPA21 when anti-RPA190 antibody was used for immunoprecipitation (Fig. 3*B*). These results confirm that Ker1p associates with pol I *in vivo*. No subunit was precipitated without the specific antibodies (*lane 3*). It should be noted that the bands of Ker1p again appeared to be doublets (*lane 2*), suggesting that the upper and lower bands correspond to the 32- and 30-kDa forms of the protein, respectively, as shown in Fig. 1*B*. The results suggest that pol I associates with both phosphorylated and non-phosphorylated Ker1p.

Ker1p Is Co-fractionated Biochemically with pol I—The above results suggest that Ker1p is a pol I subunit. To confirm biochemically that Ker1p is a novel pol I subunit, we purified pol I from an *S. pombe* strain (YI28) expressing both Ker1p-HA_3 and RPA140 tagged with a His_6-FLAG epitope. The whole cell extract was first affinity-purified using a nickel-agarose column and then fractionated by DEAE-Sephadex A25 column chromatography. We observed that Ker1p co-eluted with the peak fractions (fractions 13 and 14) of pol I detected through the RPA190 and RPA21 subunits (Fig. 4). Although more rigorous biochemical purification is needed, the elution pattern through the DEAE column confirms that Ker1p is a subunit of pol I. We noted that fractions 11 and 12 might also contain pol I without Ker1p and RPA21, but we did not examined these fractions further in this study.

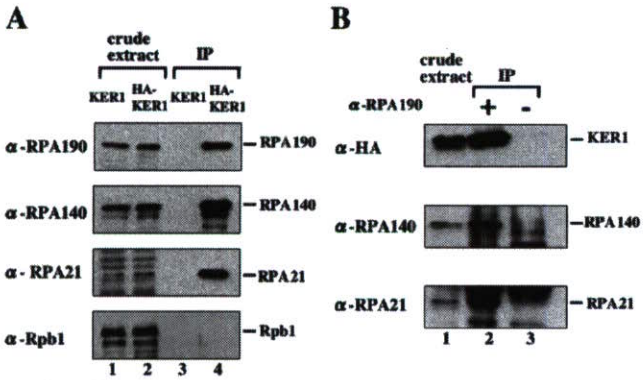

FIG. 3. **Ker1p associates with pol I.** *A*, extracts from strains IZ2 and YI28 expressing Ker1p (*KER1*) and Ker1p-HA_3 (*HA-KER1*), respectively, were immunoprecipitated with anti-HA monoclonal antibody (12CA5) beads. The extracts (*lanes 1* and *2*) and immunoprecipitates (*IP*; *lanes 3* and *4*) were subjected to SDS-PAGE, followed by immunoblot analysis with antibodies against RPA190, RPA140, RPA21, and Rpb1. 25 μg of crude extract was used for each control. *B*, extracts from strains expressing Ker1p-HA_3 were immunoprecipitated with anti-RPA190 antibody. The extract (*lane 1*), the immunoprecipitates with anti-RPA190 antibody (*lane 2*), and a sample without anti-RPA190 antibody treatment (*lane 3*) were subjected to SDS-PAGE, followed by immunoblot analysis with antibodies against HA, RPA140, and RPA21. The position of each band is indicated by the *bar* on the right of *A* and *B*. Ker1p appears as a doublet of bands. The dense bands seen at the top of the *third panel* (*lanes 2* and *3*) were derived from the light chain of immunoglobulin G.

Genetic Interaction between Ker1p and RPA21—We have previously shown that overproduced Rrn3p is able to suppress the temperature-sensitive growth defect of *rpa21* mutants, indicating a genetic interaction between RPA21 and Rrn3p (41). To examine the genetic interaction between Ker1p and RPA21, we introduced a multicopy vector expressing Ker1p under the control of the CMV promoter into the three temperature-sensitive *rpa21* mutants (*ts152*, *ts296*, and *ts2817*) (41) and examined whether the growth defects of the mutants were suppressed at the restrictive temperature. As shown in Fig. 5, overproduction of Ker1p clearly suppressed the growth deficiency of the three mutants, indicating a genetic interaction between Ker1p and RPA21. Since A14 was shown previously to be required for stable association of A43 with pol I in *S. cerevisiae* (11), it appears that Ker1p is also required for stable association of RPA21 with pol I.

Ker1p Has a Limited Homology to S. cerevisiae A14—No apparent homologous protein was initially found when the Ker1p sequence was used in a data base search. However, the results obtained above clearly indicate that Ker1p is a pol I subunit and that it interacts with RPA21. Because RPA21 is an ortholog of A43 of *S. cerevisiae*, we re-examined the homology of Ker1p to *S. cerevisiae* A14, which heterodimerizes with A43. Previously, A14 was suggested to have homology to a putative open reading frame of IPF1568 from *Candida albicans* (11), suggesting that the A14 gene family is conserved in *C. albicans*, although no genetic or biochemical evidence was presented. This suggestion prompted us to directly investigate the homologies among Ker1p, A14, and IPF1568 (hereafter referred to as *C. albicans* A14), and Fig. 6 shows an alignment of these proteins constructed using ClustalW. We found that Ker1p shows 21% identity and 27% similarity to the 126-amino acid sequence of *S. cerevisiae* A14 and that the N-terminal 60 amino acids of Ker1p show especially high identity (37%) and similarity (43%) to *S. cerevisiae* A14. The N-terminal region also shows significant identity between the A14 subunits of *S. cerevisiae* and *C. albicans* (11), and Ker1p shows 26% identity and 36% similarity to the 132-amino acid sequence of *C. albicans* A14. The local identity of Ker1p to the *S. cerevisiae* and *C. albicans* A14 subunits is especially high (38 and 42%, respectively) between amino acids 42 and 65 of Ker1p, and this region contains a motif that may be conserved between the *S. cerevisiae* and *C. albicans* A14 subunits (SQLKRIQR), as already suggested by Peyroche *et al.* (11). We conclude from these results that Ker1p is an ortholog of A14 from both *S. cerevisiae* and *C. albicans*.

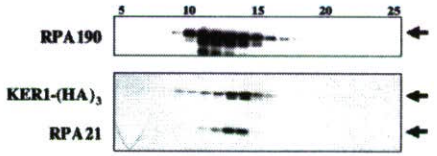

FIG. 4. **Ker1p co-fractionates with pol I.** Extracts from strains expressing Ker1p-HA_3 (*KER1-(HA)*$_3$) were loaded onto a nickel-agarose column. The eluted fractions were then loaded onto a DEAE-Sephadex A25 column and eluted with a linear gradient of 50–500 mM ammonium sulfate. Peaks of RPA190, RPA21, and Ker1p were detected by Western blotting using antibodies against RPA190, RPA21, and HA, respectively. The *numbers* indicate the *lanes*, and the *arrows* indicate RPA190, Ker1p-HA_3, and RPA21.

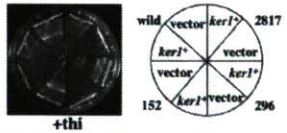

FIG. 5. **Overproduction of Ker1p suppresses the temperature-sensitive growth of three *rpa21* mutants.** Each of the temperature-sensitive mutants (*ts152*, *ts296*, and *ts2817*) transformed with pYI195 (*ker1*$^+$) or pAUR222 (*vector*) was re-streaked on minimal medium with thiamine (+*thi*) containing aureobasidin A and incubated for 5 days at 36 °C. *ker1*$^+$ was expressed under the control of the CMV promoter.

ker1$^+$ *Is Required for Growth Only at High Temperatures*—To examine whether *ker1*$^+$ is essential for cell growth, we replaced one of the chromosomal copies of *ker1*$^+$ with a disrupted *ker1*Δ::*ura4*$^+$ allele in the *S. pombe* diploid. A Ura$^+$ transformant (YI29) was chosen and subjected to tetrad analysis upon sporulation (Fig. 7*A*). Of the 20 asci dissected, one yielded four viable spores; seven yielded three viable spores; and the remaining 12 yielded two viable spores on yeast extract/peptone/dextrose medium plates at 30 °C. Large colonies were invariably Ura$^-$, whereas all of the small colonies, including the extremely small ones, were Ura$^+$. Correct disruption of the *ker1*$^+$ locus in the Ura$^+$ segregant YI30 was verified by PCR (data not shown). Growth of the colonies was tested at 25, 30, and 36 °C; none of the Ura$^+$ colonies grew at 36 °C, but all of the Ura$^-$ colonies did, indicating that *ker1*$^+$ is not essential for cell growth at 30 or 25 °C, but is required for cell growth at 36 °C (Fig. 7*B*).

*ker1*Δ *Is Suppressed by Overproduction of RPA21 or Rrn3p*—We subsequently examined whether complete deletion of *ker1*$^+$ (*ker1*Δ) is also suppressed by overproduction of RPA21. Fig. 8 shows that overexpression of RPA21 suppressed the growth defect of *ker1*Δ, again suggesting (see Fig. 5) that Ker1p is required for stable association of RPA21 with pol I. This result also suggests that RPA21 can associate with pol I independently of Ker1p. Because the rDNA-specific transcription factor Rrn3p interacts with RPA21 (41), we also examined

FIG. 6. **Amino acid sequence alignment of *S. pombe* Ker1p (*Sp*) with *S. cerevisiae* A14 (*Sc*) and *C. albicans* IPF1568 (*Ca*).** Identical and similar residues are highlighted in *black* and *gray*, respectively. The alignment was generated with the ClustalW program using the ID matrix. (The default BLOSUM matrix yielded a different alignment, in which Ker1p appeared to be less homologous to *S. cerevisiae* A14.)

whether overexpression of Rrn3p is able to suppress the temperature-sensitive growth of *ker1Δ*. As shown in Fig. 8, overproduction of Rrn3p suppressed the temperature-sensitive phenotype of *ker1Δ*, suggesting that Ker1p interacts with Rrn3p and directly stabilizes the association of Rrn3p with pol I. However, the alternative possibility remains that overproduced Rrn3p can interact with RPA21 and perhaps stabilize the association of RPA21 with pol I without the participation of Ker1p. Fig. 8 also shows that multiple copies of *rpa190*$^+$ were unable to suppress the *ker1Δ* phenotype.

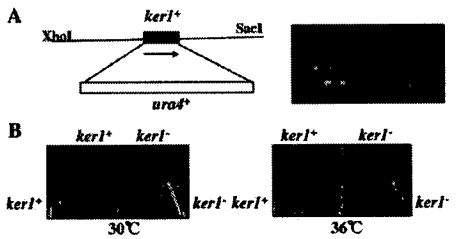

FIG. 7. **Gene disruption of *ker1*$^+$.** *A: left panel*, the 4.5-kb XhoI-SacI DNA fragment used for *ker1*$^+$ disruption; *right panel*, tetrads of diploids (*ker1Δ::ura4*$^+$*/ker1*$^+$) grown at 30 °C. *B*, growth of four haploid segregants derived from the ascospore produced by tetrad dissection of the *ker1Δ::ura4*$^+$*/ker1*$^+$ diploid.

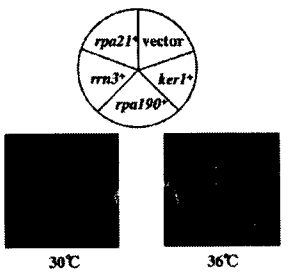

FIG. 8. **Temperature-sensitive growth of a *ker1Δ* strain is suppressed by overexpression of *rpa21*$^+$ or *rrn3*$^+$, but not *rpa190*$^+$.** *vector*, *ker1*$^+$, *rpa190*$^+$, *rrn3*$^+$, and *rpa21*$^+$ indicate strain YI28 (*ker1Δ*) carrying pREP41 (an empty vector), pYI210 (*ker1*$^+$), pGK100 (*rpa190*$^+$), pKI27 (*rrn3*$^+$), and pYI82 (*rpa21*$^+$). Each transformant was re-streaked on minimal medium plates without leucine and thiamine and incubated at 36 or 30 °C for 5 days.

Dissociation of Ker1p from pol I in Post-log-phase Cells—The data in Fig. 8 suggest that Ker1p is involved in stabilizing the association of Rrn3p with pol I, either directly or indirectly. Because Rrn3p is released from pol I in post-log-phase or growth-arrested cells (23, 24, 26), we examined whether Ker1p is also released from pol I, resulting in destabilization of Rrn3p in pol I in post-log-phase cells. As shown in Fig. 9, pol I from cells expressing Ker1p-HA$_3$ in mid- and post-log phase was immunoprecipitated with anti-RPA190 antibody, and the relative amounts of RPA190, RPA140, and Ker1p were compared. We observed a drastic decrease in the ratio of Ker1p (both phosphorylated and non-phosphorylated) to RPA190 in pol I prepared from post-log-phase cells (Fig. 9*A*, *right panels*, compare *lanes 2* and *3* with *lane 1*), although the ratio of RPA140 to RPA190 did not change significantly, suggesting that Ker1p is dissociated from pol I in the post-log phase. The dissociation of Ker1p from pol I may cause instability of Rrn3p in pol I, either directly or indirectly, resulting in dissociation of Rrn3p from pol I, which inactivates rDNA transcription.

DISCUSSION

In this study, we have shown that Ker1p isolated by a yeast two-hybrid system using RPA21 as bait is the counterpart of the *S. cerevisiae* pol I subunit A14. This is the first demonstration that a pol I-specific A14 ortholog is conserved in eukaryotes other than *S. cerevisiae*, despite no apparent homolog of A14 being identified in the *S. pombe* genome. We have successfully aligned the amino acid sequence of almost the entire length of Ker1p with those of A14 and IPF1568 (Fig. 6), indicating that these subunits are indeed grouped into a gene family. Our investigation of Ker1p has, however, also revealed features of Ker1p that are distinct from those of A14. First, Ker1p is phosphorylated (Fig. 1), whereas phosphorylation of A14 has never been observed. Second, Ker1p is suggested to interact, either directly or indirectly, with Rrn3p and to stabilize the association of Rrn3p with pol I *in vivo* (Fig. 8), whereas it is unclear whether A14 affects the stability of Rrn3p with pol I *in vivo*. Third, Ker1p is released from pol I in post-log-phase cells (Fig. 9), whereas such instability of A14 in post-log-phase or growth-arrested cells is unknown in *S. cerevisiae*. The significance of these differences must await future studies to determine whether A14 can be phosphorylated or does dissociate from pol I in post-log-phase cells.

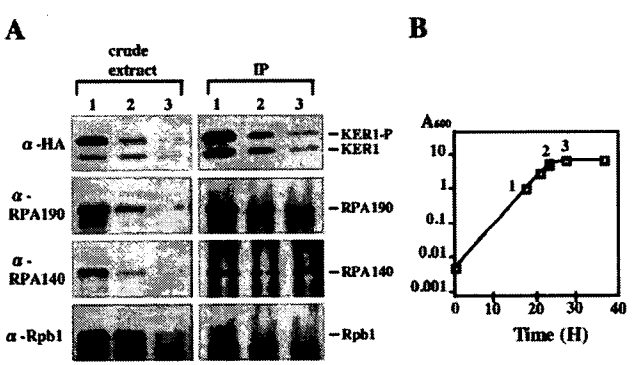

FIG. 9. **Dissociation of Ker1p from pol I in post-log-phase cells.** *A*, extracts were prepared from strain YI28 in mid-log-phase cells (*lane 1*) and post-log-phase cells (*lanes 2* and *3*) at the times indicated in *B*. *Left panels*, for detection of each subunit in the crude extract, 50 μg of each extract was loaded onto an SDS-polyacrylamide gel. Ker1p-HA$_3$, RPA190, RPA140, and Rpb1 (pol II for a control) were detected by immunoblot analysis with antibodies against HA, RPA190, RPA140, and Rpb1, respectively. *Right panels*, pol I in the crude extract was immunoprecipitated with anti-RPA190 antibody. The immunoprecipitates (*IP*) were subjected to SDS-PAGE, followed by immunoblot analysis with antibodies against HA, RPA190, RPA140, and Rpb1. We noted that bands detected by anti-Rpb1 antibody were nonspecific. *KER1-P*, phosphorylated Ker1p; *KER1*, Ker1p. *B*, strain YI28 was grown in yeast extract/dextrose medium at 30 °C. The culture was harvested at the indicated times (*time points 1, 2,* and *3*). The A_{600} values of the culture at *time points 1, 2,* and *3* were ~1.0 (mid-log phase), ~5.3, and ~6.8 (post-log phase), respectively. The doubling times at each point were ~2 h (*time point 1*), ~6 h (*time point 2*), and ~20 h (*time point 3*). In this study, we defined a temporary slow growth phase, such as those at *time points 2* and *3*, as a post-log phase.

TABLE II

Comparison of the pol I subunits of S. pombe and S. cerevisiae

The sequence data and identity were obtained as indicated: *rpa190*$^+$ (36, 37); *rpa140*$^+$ (GenBank™/EMBL accession number AL136535); *rpa42*$^+$ (38); *rpa17*$^+$ (39); *Sprpa12*$^+$ (40); *rpb5*$^+$, *rpb6*$^+$, *rpb8*$^+$, *rpb10*$^+$, and *rpb12*$^+$ (12); *rpa51*$^+$ (42); *rpa21*$^+$ (41); and *ker1*$^+$ (this work).

S. pombe		*S. cerevisiae*		Identity
Gene	No. of amino acids	Gene	No. of amino acids	
				%
rpa190$^+$	1689	*RPA190*	1664	50
rpa140$^+$	1228	*RPA135*	1203	63
rpa42$^+$	348	*RPC40*	335	58
rpa17$^+$	125	*RPC19*	142	63
Sprpa12$^+$	119	*RPA12*	125	55
rpb5$^+$	210	*RPB5*	215	56
rpb6$^+$	142	*RPB6*	155	54
rpb8$^+$	125	*RPB8*	146	39
rpb10$^+$	71	*RPB10*	70	72
rpb12$^+$	63	*RPB12*	70	39
rpa51$^+$	425	*RPA49*	415	30
rpa21$^+$	173	*RPA43*	326	36
ker1$^+$	147	*RPA14*	137	21
?		*RPA34*	233	

A comparison of the pol I subunits in *S. pombe* and *S. cerevisiae* is shown in Table II. 10 subunits constituting the core structure (RPA190, RPA140, RPA42, RPA17, Rpb5, Rpb6, Rpb8, Rpb10, Rpb12, and SpRPA12) are conserved from *S. cerevisiae* to *S. pombe* pol I. RPA190 and RPA140 were not examined, but seven of the remaining eight subunits (all except Rpb8) could substitute for the corresponding subunits in *S. cerevisiae*, suggesting functional conservation of most of the subunits (38–40, 49). In three specific subunits, including Ker1p, RPA51 was tested and found to rescue an *rpa49* mutation in *S. cerevisiae* (42). Although RPA21 encodes only 174 amino acids and appears to be much diversified from *S. cerevisiae* A43 (*S. cerevisiae* A43 contains 326 amino acids), its role in pol I recruitment to the rDNA promoter is conserved (41), and it is plausible that the N-terminal region conserved in the A43 gene family plays a role in the interaction with Rrn3p. The question of whether *S. pombe* pol I conserves a counterpart of *S. cerevisiae* A34.5 is unresolved. We believe that the primary sequence of the A34.5 homolog, if any such protein exists, may be poorly conserved in *S. pombe*. Mouse pol I has been found to contain distinct subunits from lower eukaryotes, such as PAF67 and PAF49 (33, 34, 50). These results tempt us to speculate that lower eukaryotes such as yeast might conserve the 14 subunits found in *S. cerevisiae* and that higher eukaryotes might have more specific subunits such as PAF67 and PAF49, in addition to the 14 conserved subunits.

It is known that A14 is not phosphorylated in *S. cerevisiae* pol I (1, 51, 52), whereas here Ker1p was found to be phosphorylated, suggesting that specific subunit phosphorylation has also evolved independently among pol I subunits. Indeed, *S. cerevisiae* A43 is multiphosphorylated (53), whereas mammalian A43 is barely phosphorylated (24). It has been argued that A43 must be phosphorylated to associate with Rrn3p in *S. cerevisiae*, whereas Rrn3p phosphorylation is a prerequisite for the association of A43 with Rrn3p in mammalian cells (24, 53, 54). In this context, the functional dissection of Ker1p phosphorylation/dephosphorylation may provide a novel insight into the pol I recruitment mechanism.

It appears that Ker1p is required for the stability of RPA21 based on multicopy suppression experiments. (i) *ker1Δ* exhibits a temperature-sensitive growth deficit, and the temperature-sensitive deficit is suppressed by overproduction of RPA21 (Fig. 8). (ii) The temperature-sensitive growth deficit of three *rpa21* mutants (*ts152*, *ts296*, and *ts2817*) is suppressed by overexpression of *ker1*$^+$ (Fig. 5). Since it is known that A14 is also required for the stability of A43 in *S. cerevisiae* (9, 11), the role of Ker1p may be, as expected, similar to that of A14. To verify the Ker1p function, purification of pol I from extracts of *ker1Δ* mutants deserves future study. Unexpectedly, as shown in Fig. 8, overproduction of Rrn3p also suppresses the temperature-sensitive phenotype of the *ker1Δ* mutant, suggesting that Ker1p is also required for the stable association of Rrn3p with pol I. Alternatively, these suppression data could suggest that overproduction of Rrn3p suppresses the instability of RPA21 in pol I without participation of Ker1p, leading to indirect suppression of the temperature-sensitive phenotype of *ker1Δ*. Clearly, future biochemical experiments are required to reveal whether Rrn3p directly interacts with Ker1p.

Accumulating evidence has shown that dissociation of Rrn3p from pol I in post-log-phase or growth-arrested cells causes a decrease in pol I recruitment to the promoter, resulting in a decrease in or halting of rDNA transcription. As described above, it has been argued that post-translational modification (phosphorylation/dephosphorylation) of A43 and Rrn3p regulates the stability of the pol I-Rrn3p complex, causing dissociation of Rrn3p from pol I in post-log-phase or growth-arrested cells. The immunoprecipitation experiments in Fig. 9, performed using anti-RPA190 antibody, showed that the amounts of both forms of Ker1p (phosphorylated and non-phosphorylated forms) relative to RPA140 and RPA190 are reduced drastically after cells enter the post-log phase. The results suggest that dissociation of Ker1p from pol I in post-log-phase cells is one of the regulatory mechanisms of Rrn3p dissociation from pol I since the dissociation of Ker1p may lead to instability of RPA21 and Rrn3p in pol I. It is also possible that release of Ker1p induces certain modification(s) of RPA21 and Rrn3p that result in release of Rrn3p from pol I. Therefore, it is tempting to speculate that the association/dissociation of Ker1p might primarily regulate growth-dependent transcription of rDNA in *S. pombe*.

Acknowledgments—We acknowledge the Resource Center/Primary Database of the German Human Genome Project for sending us a cosmid including *rrn3*$^+$. We thank L. Pape (University of Wisconsin) for communicating the results of a homology search for Ker1p. We also acknowledge Akio Toh-e (University of Tokyo) for critical reading of the manuscript.

REFERENCES

1. Thuriaux, P., and Sentenac, A. (1992) in *The Molecular and Cellular Biology of the Yeast Saccharomyces* (Jones E. W., Pringle J. R., and Broach J. R., eds) Vol. 2, pp. 1–48, Cold Spring Harbor Laboratory, Cold Spring Harbor, NY
2. Armache, K. J., Kettenberger, H., and Cramer, P. (2003) *Proc. Natl. Acad. Sci. U. S. A.* **100**, 6964–6968
3. Bushnell, D. A., and Kornberg, R. D. (2003) *Proc. Natl. Acad. Sci. U. S. A.* **100**, 6969–6973
4. Bischler, N., Brino, L., Carles, C., Riva, M., Tschochner, H., Mallouh, V., and Schultz, P. (2002) *EMBO J.* **21**, 4136–4144
5. Edwards, A. M., Kane, C. M., Young, R. A., and Kornberg, R. D. (1991) *J. Biol. Chem.* **266**, 71–75
6. Thuriaux, P., Mariotte, S., Buhler, J. M., Sentenac, A., Vu, L., Lee, B. S., and Nomura, M. (1995) *J. Biol. Chem.* **270**, 24252–24257
7. Liljelund, P., Mariotte, S., Buhler, J. M., and Sentenac, A. (1992) *Proc. Natl. Acad. Sci. U. S. A.* **89**, 9302–9305
8. Gadal, O., Mariotte-Labarre, S., Chedin, S., Quemeneur, E., Carles, C., Sentenac, A., and Thuriaux, P. (1995) *Mol. Cell. Biol.* **17**, 1787–1795
9. Smid, A., Riva, M., Bouet, F., Sentenac, A., and Carles, C. (1995) *J. Biol. Chem.* **270**, 13534–13540

10. Peyroche, G., Milkereit, P., Bischer, N., Tschochner, H., Schultz, P., Sentenac, A., Carles, C., and Riva, M. (2000) *EMBO J.* **19,** 5473–5482
11. Peyroche, G., Levillain, E., Siaut, M., Callebaut, I., Schultz, P., Sentenac, A., Riva, M., and Carles, C. (2002) *Proc. Natl. Acad. Sci. U. S. A.* **99,** 14670–14675
12. Sakurai, H., Mitsuzawa, H., Kimura, M., and Ishihama, A. (1999) *Mol. Cell. Biol.* **19,** 7511–7518
13. Siaut, M., Zaros, C., Levivier, E., Ferri, M. L., Court, M., Werner, M., Callebaut, I., Thuriaux, P., Sentenac, A., and Conesa, A. (2003) *Mol. Cell. Biol.* **23,** 195–203
14. Todone, F., Brick, P., Werner, F., Weinzierl, R. O. J., and Onesti, S. (2001) *Mol. Cell* **8,** 1137–1143R. O. J.
15. Sheffer, A., Varon, M., and Choder, M. (1999) *Mol. Cell. Biol.* **19,** 2672–2680
16. Lanzendorfer, M., Smid, A., Klinger, C., Schultz, P., Sentenac, A., Carles, C., and Riva, M. (1997) *Genes Dev.* **11,** 1037–1047
17. Orlicky, S., Tran, P. T., Sayre, M. H., and Edwards, A. M. (2001) *J. Biol. Chem.* **276,** 10097–10102
18. Meka, H., Daoust, G., Arnvig, K. B., Werner, F., Brick, P., and Onesti, S. (2003) *Nucleic Acids Res.* **31,** 4391–4400
19. Ferri, M. L., Peyroche, G., Siaut, M., Lefebvre, Q., Carles, C., Conesa, C., and Sentenac, A. (2000) *Mol. Cell. Biol.* **20,** 488–495
20. Moss, T., and Stefanovsky, V. Y. (2002) *Cell* **109,** 545–548
21. Ju, Q., and Warner, J. R. (1994) *Yeast* **10,** 151–157
22. Zaragoza, D., Ghavidel, A., Heitman, J., and Schultz, M. (1998) *Mol. Cell. Biol.* **18,** 4463–4470
23. Bodem, J., Dobreva, G., Hofmann-Rohrer, U., Iben, S., Zentgraf, H., Delius, H., Vingron, M., and Grummt, I. (2000) *EMBO Rep.* **1,** 171–175
24. Cavanaugh, A. H., Hirschler-Laszkiewicz, I., Hu, Q., Dundr, M., Smink, T., Misteli, T., and Rothblum, L. I. (2002) *J. Biol. Chem.* **277,** 27423–27432
25. Yamamoto, R. T., Nogi, Y., Dodd, J. A., and Nomura, M. (1996) *EMBO J.* **15,** 3964–3973
26. Milkereit, P., and Tschochner, H. (1998) *EMBO J.* **17,** 3692–3703
27. Keener, J., Josaitis, C. A., Dodd, J. A., and Nomura, M. (1998) *J. Biol. Chem.* **273,** 33795–33802
28. Miller, G., Panov, K. I., Friedrich, J. K., Trinkle-Mulcahy, L., Lamond, A. I., and Zomerdijk, J. C. B. M. (2001) *EMBO J.* **20,** 1373–1382J. C. B. M.
29. Claypool, J. A., French, S. L., Johzuka, K., Eliason, K., Vu, L., Dodd, J. A., Beyer, A. L., and Nomura, M. (2004) *Mol. Biol. Cell* **15,** 946–956
30. Grummt, I. (2003) *Genes Dev.* **17,** 1691–1702
31. Woychik, N. A. (1998) *Cold Spring Harbor Symp. Quant. Biol.* **63,** 311–317
32. Hu, P., Wu, S., Sun, Y., Yuan, C., Kobayashi, R., Myers, M. P., and Hernandez, N. (2003) *Mol. Biol. Cell* **22,** 8044–8055
33. Seither, P., Iben, S., Thiry, M., and Grummt, I. (2001) *Biol. Chem.* **382,** 1163–1170
34. Yamamoto, K., Yamamoto, M., Hanada, K., Nogi, Y., Matsuyama, T., and Muramatsu, M. (2004) *Mol. Cell. Biol.* **24,** 6525–6535
35. Alfa, C., Fantes, P., Hyams, J., McLeod, M., and Warbrick, E. (1993) *Experiments with Fission Yeast*, Cold Spring Harbor Laboratory , Cold Spring Harbor, NY
36. Yamagishi, M., and Nomura, M. (1988) *Gene (Amst.)* **74,** 503–515
37. Hirano, T., Konoha, G., Toda, T., and Yanagida, M. (1989) *J. Cell Biol.* **108,** 243–253
38. Imazawa, Y., Imai, K., Fukushima, A., Hisatake, K., Muramatsu, M., and Nogi, Y. (1999) *Mol. Gen. Genet.* **262,** 749–757
39. Imai, K., Imazawa, Y., Yao, Y., Yamamoto, K., Hisatake, K., Muramatsu, M., and Nogi, Y. (1999) *Mol. Gen. Genet.* **261,** 364–373
40. Imazawa, Y., Imai, K., Yao, Y., Yamamoto, K., Hisatake, K., Muramatsu, M., and Nogi, Y. (2001) *Mol. Gen. Genet.* **264,** 852–859
41. Imazawa, Y., Hisatake, K., Nakagawa, K., Muramatsu, M., and Nogi, Y. (2002) *Genes Genet. Syst.* **77,** 147–157
42. Nakagawa, K., Hisatake, K., Imazawa, Y., Ishiguro, A., Matsumoto, M., Pape, L., Ishihama, A., and Nogi, Y. (2003) *Genes Genet. Syst.* **78,** 199–209
43. Sherman, F., Fink, G. R., and Hicks, J. B. (1986) *Laboratory Course Manual for Methods in Yeast Genetics*, pp. 163–167, Cold Spring Harbor Laboratory, Cold Spring Harbor, NY
44. Harper, J. W., Adami, G. R., Wei, N., Keyomarsi, K., and Elledge, S. J. (1993) *Cell* **75,** 805–816
45. Mitsuzawa, H., Seino, H., Yamao, F., and Ishihama, A. (2001) *J. Biol. Chem.* **276,** 17117–17124
46. Ishiguro, A., Nogi, Y., Hisatake, K., Muramatsu, M., and Ishihama, A. (2000) *Mol. Cell. Biol.* **20,** 1263–1270
47. Sawin, K. E., and Nurse, P. (1996) *Proc. Natl. Acad. Sci. U. S. A.* **94,** 15146–15151
48. Oakes, M., Nogi, Y., Clark, M. W., and Nomura, M. (1993) *Mol. Cell. Biol.* **13,** 2441–2455
49. Shpakovski, G. V., Gadal, O., Labarre-Mariotte, S., Lebedenko, E. N., Miklos, I., Sakurai, H., Proshkin, S. A., Van Mullem, V., Ishihama, A., and Thuriaux, P. (2000) *J. Mol. Biol.* **295,** 1119–1127
50. Yuan, X., Zhao, J., Zentgraf, H., Hommer-Rohrer, U., and Grummt, I. (2002) *EMBO Rep.* **3,** 1082–1087
51. Buhler, J. M., Iborra, F., Sentenac, A., and Fromageot, P. (1976) *FEBS Lett.* **71,** 37–41
52. Breant, B., Buhler, J. M., Sentenac, A., and Fromageot, P. (1983) *Eur. J. Biochem.* **130,** 247–251
53. Fath, S., Milkereit, P., Peyroche, G., Riva, M., Carles, C., and Tschochner, H. (2001) *Proc. Natl. Acad. Sci. U. S. A.* **98,** 14334–14339
54. Zao, J., Yuan, X., Frodin, M., and Grummt, I. (2003) *Mol. Cell* **11,** 405–413
55. Waddel, S., and Jenkins, J. R. (1995) *Nucleic Acids Res.* **23,** 1836–1837
56. Basi, G., Schmid, E., and Maundrell, K. (1993) *Gene (Amst.)* **123,** 131–136

Glutathione S-transferase theta 1 expressed in granulosa cells as a biomarker for oocyte quality in age-related infertility

Megumu Ito, M.D.,[a] *Miho Muraki, B.S.,*[a,f] *Yuji Takahashi, Ph.D.,*[a] *Misa Imai, M.S.,*[a] *Tohru Tsukui, Ph.D.,*[b] *Naomi Yamakawa, Ph.D.,*[c] *Koji Nakagawa, M.D.,*[a] *Shirei Ohgi, M.D.,*[a] *Takashi Horikawa, M.D.,*[a] *Wakako Iwasaki, M.D.,*[a] *Ayumi Iida, B.S.,*[a] *Yoshihiro Nishi, M.D.,*[d] *Toshihiko Yanase, M.D.,*[e] *Hajime Nawata, M.D.,*[e] *Kenji Miyado, Ph.D.,*[a] *Tomohiro Kono, Ph.D.,*[f] *Yoshihiko Hosoi, Ph.D.,*[g] *and Hidekazu Saito, M.D.*[a]

[a] Division of Reproductive Medicine, Department of Perinatal Medicine and Maternal Care, National Center for Child Health and Development, Tokyo, Japan; [b] Research Center for Genomic Medicine, Saitama Medical University, Saitama, Japan; [c] Research Team for Geriatric Diseases, Tokyo Metropolitan Institute of Gerontology, Tokyo, Japan; [d] Department of Physiology, Kurume University, Kurume, Japan; [e] Department of Medicine and Bioregulatory, Graduate School of Medical Science, Kyushu University, Fukuoka, Japan; [f] Department of BioScience, Tokyo University of Agriculture, Tokyo, Japan; and [g] Division of Biological Science, Graduate School of Biology-Oriented Science and Technology, Kinki University, Wakayama, Japan

Objective: The goal of this study was to identify a reliable biomarker for age-related infertility.
Design: Laboratory study.
Setting: ART laboratory.
Patient(s): Patients undergoing intracytoplasmic sperm injection or IVF cycles.
Intervention(s): Expression of Glutathione S-transferase (GST) mRNA and protein in mural and cumulus granulosa cells obtained from infertile patients were examined by reverse transcriptase-polymerase chain reaction and immunofluorescence.
Main Outcome Measure(s): Correlation between the expression of GST theta 1 (GSTT1) in granulosa cells and oocyte quality was a main outcome measure.
Result(s): Expression of GSTT1 in granulosa cells from male factor patients was positively correlated with age and negatively with cumulus-oocyte complex maturity. When samples with high and low GSTT1 in granulosa cells were extracted from the other infertility factors, cumulus-oocyte complex maturity in the high GSTT1 group was significantly lower than that in the low GSTT1 group (high: 27.2% vs. low: 51.3%). The developmental capacity of oocytes in the high GSTT1 group was likely to be lower (high: 26.4% vs. low: 43.9%). Up-regulation of GSTT1 during aging may be promoted by FSH and H_2O_2, determined by an in vitro model.
Conclusion(s): GSTT1 is a good indicator for age-related infertility. (Fertil Steril® 2007;■:■–■. ©2007 by American Society for Reproductive Medicine.)

Key Words: Glutathione S-transferase theta 1 (GSTT1), aging, granulosa cell, biomarker, oocyte quality

Maternal age is a risk factor for infertility. The decline in fecundity becomes clinically evident when women reach their mid-30s (1). Despite the disadvantages, women in Western industrialized nations now tend to delay the birth of their first child until a later age than before. This tendency leads to declining birth rates, resulting in aging populations, which is a serious social issue. Although the exact mechanism by which aging causes female reproductive disorders is unclear, age-related changes in the ovary—including hormonal imbalance (2), decrease of the ovarian follicle pool (3), increase of oocyte aneuploidy (4), and mitochondrial dysfunction in oocytes (5)—account for the loss of reproductive function.

Oxidative stress is a major source of aging; it damages genomic and mitochondrial DNA, causing tumors and/or apoptosis in many cell types. Oocytes and somatic cells stored in ovaries are thought to be exposed to reactive oxygen species (ROS) during both ovulation and aging (6). In mice, repeated ovarian stimulation with gonadotropins increased the

Received April 3, 2007; revised July 6, 2007; accepted July 30, 2007.
M. Ito, M. Muraki, and Y. Takahashi contributed equally to this work.
Partly supported by a grant of Research on Child Health and Development (2005–2008) from the Ministry of Health, Labour and Welfare, and partly by grants (2005–2008: #17791147, #17791148; 2006–2009: #18591818) from the Ministry of Education, Culture, Sports, Science and Technology.
Reprint requests to: Yuji Takahashi, Ph.D., Division of Reproductive Medicine, Department of Perinatal Medicine and Maternal Care, National Center for Child Health and Development, 2-10-1 Okura, Setagaya-ku, Tokyo 157-8535, Japan (FAX: +81-3-3416-2222; E-mail: takahashi-yj@ncchd.go.jp).

0015-0282/07/$32.00
doi:10.1016/j.fertnstert.2007.07.1389

incidence of oxidative DNA damage and mitochondrial DNA mutation (7). In humans, accumulation of 8-hydroxy-2'-deoxyguanine, a byproduct of oxidative stress-induced digestion of DNA, in mural and cumulus granulosa cells from infertile patients correlated negatively with the oocyte quality (8). Moreover, the amount of ROS in human follicular fluid was negatively correlated with oocyte development potential (9). The apoptotic status of rat follicular cells was also in parallel with ROS production (10). In agreement with this report, apoptosis possibly induced by ROS in granulosa cells from infertile patients was closely related to the oocyte quality (11, 12). Thus, repeated exposure of oocytes and granulosa cells to oxidative stress must be associated with reproductive failure.

Organisms have many adaptive devices to oxidative stress and genotoxins. Glutathione S-transferases (GSTs) are well known to detoxify the metabolites of genotoxic molecules to more water-soluble and readily excretable forms. In addition, they are known to protect cells from ROS-induced membrane lipid peroxidation (13). Because of their roles in self-defense, mutations of GSTs are often linked to certain diseases. Several studies have indicated that GSTs may play a role in predisposition to cancer, with the GSTM1 and GSTT1 null phenotypes (14–16). A number of common polymorphisms affect enzyme activity; these include gene deletions in the GSTM1 and GSTT1 genes, which result in lack of the corresponding enzyme activity (17). The mutated products modulate chemical binding to DNA, and are associated with myocardial infarction as well as the tobacco-related cancers in smokers (18, 19). In addition, polymorphisms of GSTM1 and GSTT1 may increase the risk of recurrent pregnancy loss (20), and susceptibility to polycystic ovaries (21).

Because of the limited availability of molecular information and biomarkers for age-related infertility, effective diagnosis and therapy have not yet been established. The aim of our present study, therefore, was to explore the possibility that the expression of GSTs in granulosa cells obtained from infertility patients is associated with age-related changes of fecundity. We screened for the expression of GSTs in young or older (stressed) granulosa cells by reverse transcriptase-polymerase chain reaction (RT-PCR) analysis, to select GSTs as potential biomarkers for age-related infertility; we then compared the expression levels of each potential molecule in various patients with oocyte quality. Finally, we examined the cause of aberrant expression of GSTs in in vitro model systems.

MATERIALS AND METHODS

Reagents

Hoechst 33342, human FSH, human LH, and hCG were purchased from Sigma Chemical Co. (St. Louis, MO). Rabbit polyclonal antibodies against GSTT1 and BAX were purchased from Santa Cruz Biotechnology Inc. (Santa Cruz, CA). Donkey anti-rabbit IgG-Cy3 was purchased from Chemicon International Co. Ltd. (Temecula, CA).

Patients and Samples

Mural granulosa cells and cumulus granulosa cells were obtained from infertile patients undergoing IVF/intracytoplasmic sperm injection cycles between September 2004 and June 2007 at the National Center for Child Health and Development, Japan. One hundred seventy-six infertile patients (male factor: 50; tubal factor: 32; unknown factor: 94) participated in the study. The institutional review board approved the experiments on these samples, and individual patients provided prior informed consent.

Mural granulosa cells were isolated from follicular aspirates and washed three to four times in phosphate-buffered saline (PBS) containing 1 mg/mL bovine serum albumin (BSA) (PBS + BSA). In addition, cumulus-oocyte complexes (COCs) were isolated and washed twice in IVF medium (human tubal fluid medium purchased from Irvine Scientific Co., Santa Ana, CA). Cumulus cells were then detached from the COCs physically using 27-G fine needles in IVF medium and washed three times in PBS + BSA. Just before detachment of the cumulus cells, the maturity of the COCs was evaluated based on the following morphologic criteria: [1] complete expansion of cumulus with visible halo (mature), [2] incomplete expansion of cumulus without halo (immature), and [3] incomplete or complete expansion and dissociation of cumulus with dark spots (dysmature).

A portion of the mural and cumulus granulosa cells was transferred into 1.5-mL microtubes, centrifuged for 10 minutes at 15,000 rpm at 4°C to remove excess buffer, and stored at −80°C until use. The remaining samples were fixed in 4% formaldehyde in PBS + BSA for 30 minutes at room temperature, washed three times in PBS + BSA, put on glass slides, air-dried, and stored at 4°C until use.

Preparation of Mouse Ovaries

Experiments were approved by the Animal Ethics Committee at the National Center for Child Health and Development. ICR female mice (8 weeks old) were purchased from Sankyo Labo Service Co. Ltd (Tokyo, Japan). They were injected with 6 IU of pregnant mare serum gonodotropin (PMSG), and ovaries were collected at 72 hours post-injection to induce the atretic follicles. In addition, some mice were injected with 6 IU hCG following PMSG administration, and ovaries were collected at 8 hours post-hCG injection to obtain ovaries with preovulatory follicles. Those ovaries were then fixed in 4% paraformaldehyde in PBS overnight at 4°C. They were then sectioned serially by Cryostat (8 μm interval, Leica Microsystems Japan Co. Ltd, Tokyo, Japan), and subjected to immunofluorescence studies. The sections were kept at 4°C until use.

Cell Culture and Treatment

A human granulosa-like tumor cell line, KGN, was established previously (22). The cells were maintained in Dulbecco's minimum essential medium/Ham's F12 medium supplemented with 10% heat-inactivated fetal calf serum, 100 μg/mL penicillin, and 100 IU/mL streptomycin at 37°C in a CO_2 incubator. For the immunofluorescence study, the cells were seeded onto eight-well culture slides (BD Japan Co. Ltd, Tokyo, Japan) and stimulated with either gonadotropins (FSH, LH, hCG) or oxidative stress (H_2O_2, 10 μM) for 6 to 24 hours at the indicated concentration. The cells were incubated in serum-free culture medium for 2 hours before treatment with the various stimuli.

Semiquantitative RT-PCR Analysis

Total RNA was isolated from mural granulosa cells using ISOGEN RNA extraction reagent (Nippon Gene Co. Ltd., Tokyo, Japan). The first-strand cDNA of each sample was synthesized from 1 μg total RNA using SuperScript III reverse transcriptase (Invitrogen Corp., Carlsbad, CA), according to the manufacturer's instructions. Expression of GSTs was then monitored by PCR amplification. The primers and cycles used for each gene are as follows; GSTA1 F: GATTTGTTTTCATTAGGATCTGA, R: CATGGAGAAGA TTGGAAATCTGAAT, 32 cycles; GSTA2 F: CAGCCACA AAGGTGACAGCA, R: TCAGGTTGAGTAAAGGGCAG, 32 cycles; GSTA3 F: GGTGGCCTTGAGAAGCTGAG, R: TGGTTTCTTTGAGTAAAGTCT, 35 cycles; GSTA4 F: GGCTATAATTAGATACTTTCCTGTG, R: GGGATATT ACTTAGTTTCACTGTGT, 28 cycles; GSTCD1 F: CTTTAT CATACAAGGAACACATGAT, R: ACGGAGTATCCACAT TCTTCT, 32 cycles; GSTCD2 F: CTTTGAAATAAACTTT CAAGACTCAG, R: AAGATACCAAAAGAATATGCTCA, 32 cycles; GSTK1 F: GTATCAGAATATCTGGAACATCAA C, R: CTTTAAGTCATTTGCCATGTATAGT, 28 cycles; GSTM1 F: AAGCTATGAGGAAAAGAAGTACAC, R: ATA GACGAGAAAATCTACAAAAGTG, 28 cycles; GSTM2 F: AAGGAGCAGATTCGCGAAGAC, R: GCCTGCAGGT ATTCTGGTTTC, 28 cycles; GSTM3 F: CCCCCTTATGTA GGGTATAAAG, R: TCATAAGAGGTATCCGTGAACT, 35 cycles; GSTM4 F: ATCTTACTCCTTCCAGCCAGT, R: ACATGATGCTGGTTGGTGTC, 32 cycles; GSTM5 F: GATTACTACAGAAAGGTGCTCTG, R: TATCTAGATC AGGGAAGTCTATCAG, 32 cycles; GSTO1 F: GATCTTAG AGTTGTTTTCTAAGGTG, R: TTCTTATTAGTCAGAAC CTCCTCTA, 28 cycles; GSTO2 F: ACCACTACCGGTTCC TCTTT, R: GTGATCCTACCCGCCAACTA, 42 cycles; GSTP F: ATCTCCCTCATCTACACCAACTAT, R: AGTCC AGCAGGTTGTAGTCAG, 28 cycles; GSTT1 F: GGATCTG ATTAAAGGTCAGCACTTA, R: ACCAGTAGTCAGGGA CCTTATATTT, 35 cycles; GSTT2 F: AACAAGGATTCA TTCTGTTACTTAC, R: TTACTGATTTGTAGGAGCTCTT TAT, 32 cycles; GSTZ1 F: ATATACTGTGTAGGAGACG AGGTG, R: CGTCACATAGATAACAGTATTCCT, 32 cycles; MGST1 F: ACCTGTAAAGAAAATCATACAACTC, R: CCTCCTACCTAAAATCTAAGAAAGT, 28 cycles; MGST2 F: GTGTGGAGTTTTATCCTATATTCAT, R: CAT TAAAGGGAAGAGAAAAAGTTAG, 28 cycles; MGST3 F: AAGAAGTACAAAGTGGAGTATCCTA, R: GTAATAG CCATAAGCATAAAGAACT, 28 cycles; G3PDH F: ACCAC AGTCCATGCCATCAC, R: TCCACCACCCTGTTGCTGT A, 28 cycles. The conditions for PCR amplification were: initial denaturation at 94°C for 5 minutes, followed by the indicated cycles of denaturation 94°C for 45 seconds, annealing at 57°C for 45 seconds, and elongation at 72°C for 1 minute, with a final extension at 72°C for 15 minute.

The PCR products were separated on a 4% agarose gel and stained with ethidium bromide. Digital photographs were taken on a transilluminator and saved as JPEG files. The averaged band intensity was measured using Adobe Photoshop Element 2 software and the background was subtracted. Semiquantitative data on the expression level of each gene were obtained from values that had been divided by those for G3PDH.

Immunofluorescence

Mural and cumulus granulosa cells prepared as described above were permeabilized with 0.1% Triton X-100 (TX100) in PBS for 30 minutes at room temperature and blocked with 100% Blockace (Snow Brand Milk Products Co., Tokyo, Japan) overnight at room temperature. Cryosections were also blocked with 100% Blockace. The samples were treated with the first antibody at 20 μg/mL for 2 hours at room temperature, washed three times with PBS, and visualized with anti-rabbit IgG–Cy3 diluted at 1:500 in PBS + 0.1% TX100 for 2 hours at room temperature. To count the number of cells, Hoechst 33342 was loaded at 10 μM in PBS + 0.1% TX100 during treatment with the secondary antibody. The samples were then washed three times with PBS, immersed in Vectashield (Vector Laboratories Inc., Burlingame, CA), and covered with coverslips. Microphotographs were taken under an epifluorescence microscope (IX-71; Olympus, Tokyo, Japan) equipped with a computational CCD camera (CoolSnap HQ; Nippon Roper Industries, Tokyo, Japan). Photographs taken from five different areas of each sample were analyzed with MetaMorph software (Molecular Devices Corp., Tokyo, Japan), and the averaged fluorescence intensity in each image was measured. The fluorescence intensity was normalized with the number of cells in the same image to obtain the indexed fluorescence intensity per cell.

Statistical Analysis

Normalized data on the expression of GSTT1 mRNA and protein were presented as means with SEM from three to five independent experiments. Correlation between GSTT1 mRNA expression and oocyte quality (cumulus maturity and developmental capacity) was estimated by Pearson's coefficients of contingence. Expression of GSTT1 or BAX protein in mural and cumulus granulosa cells from young patients was compared with that of older patients using Student's t test or modified t test (Welch's correction). The expression levels of GSTT1 protein in KGN cells with various treatments were analyzed with one-way analysis of variance followed with Student's t test. Differences were considered statistically significant when $P<.05$. All statistical analyses were performed using Microsoft Excel software.

RESULTS

Up-regulation of GSTT1 in Mural Granulosa Cells with Aging

In most cases of male factor infertility, female fecundity is considered normal. Accordingly, oocyte quality in the women with male factor must be affected by aging. We therefore tried to select a typical age sample from 50 male factor patients, considering the age of patients and the availability of granulosa cells for the subsequent experiments. The demographic data on the patients participating in this study are summarized in Table 1.

Unlike most GSTs, GSTT1 was found to be up-regulated in aged mural granulosa cells (Fig. 1A). To explore the possibility that GSTT1 might be useful as a biomarker of age-related infertility, the correlation between GSTT1 mRNA expression in granulosa cells from male factor patients and the age of the patients was analyzed (N = 43). As shown in Figure 1B, a positive correlation between GSTT1 level and age was observed ($r = 0.36$, $P<.05$). Immunofluorescence analysis of GSTT1 in mural granulosa cells revealed that the aged cells expressed GSTT1 about 10-fold more strongly than young cells (Fig. 1C; young: 25–34 years, N = 9; aged: 38–43 years, N = 12, $P<.01$). A similar tendency was observed in cumulus granulosa cells (Fig. 1D; young: 25–34 years, N = 7; aged: 37–42 years, N = 5), although the difference was not statistically significant. These results demonstrate that GSTT1 in granulosa cells was up-regulated by aging.

GSTT1 Predicts Oocyte Quality

Because GSTT1 was shown to be a marker for aging, we next analyzed the correlation between GSTT1 expression in male factor patients and oocyte quality (number of oocytes retrieved, COC maturity, fertilization rate, and developmental rate). A negative correlation between GSTT1 mRNA expression and COC maturity was observed (Fig. 2A; $r = -0.31$, $P<.05$). Immunofluorescence revealed that GSTT1 protein in cumulus cells from the immature and dysmature COCs was up-regulated significantly compared with that from the mature COCs (Fig. 2B; N = 5, mature vs. immature, $P<.05$; mature vs. dysmature, $P<.01$). These results demonstrate that GSTT1 was an indicator for the COC maturity.

Although the COC maturity is not related to the nuclear maturity of oocytes, it may represent the apoptotic status of cumulus cells. Therefore, expression of the BAX protein, an apoptosis marker, in cumulus cells was examined by immunofluorescence. BAX expression was greatest in the dysmature cumulus cells, modest in the immature cells, and least in the mature cells (Fig. 2C; N = 6, mature vs. dysmature: $P<.05$). Supportively, both GSTT1 and BAX were expressed very strongly in mouse atretic follicles, whereas the minimum fluorescence of those molecules was seen in granulosa cells in preovulatory follicles (Fig. 2D). These results suggest that GSTT1 was an indicator for the apoptosis of the granulosa cells.

The correlation between GSTT1 expression and oocyte capacity for fertilization and development could not be examined in the male factor patients because these are affected by sperm quality. We therefore tested the expression of GSTT1 mRNA in the mural granulosa cells from other infertile patients (tubal and unknown factors), and compared this with oocyte capacities. In these cases, GSTT1 expression showed no correlations with COC maturity (Fig. 3A) or oocyte capacity for fertilization (data not shown) or development, possibly because GSTT1 expression was affected not only by aging but also by various other factors. However, when patients with high (more than the G3PDH level) or low (<1/5 of the G3PDH level) expression of GSTT1 in granulosa cells were extracted, a negative correlation between GSTT1 expression and COC maturity was observed ($r = -0.35$, $P<.05$; data not shown). The average rate of COC maturity in the group with high GSTT1 was also significantly lower than that in the group with low GSTT1 (Fig. 3B; low: 51.3%, N = 25; high: 29.5%, N = 17, $P<.01$). Therefore, defining the threshold of GSTT1 expression could be effective for extraction of the aging factor in infertile patients. In the

TABLE 1

Demographic data of IVF/ICSI patients.

		Selected samples for GST screening[d]	
	All samples	Young	Aged
Age (years)	37.3 ± 0.4	28	36
Cases of each cause			
Male factors	50		
Tubal	32		
Unknown	94		
Day 3 FSH (mIU/mL)	5.3 ± 0.2	2.5	5.1
No. of hMG ampoules[a]	23.7 ± 0.6	17	28
No. oocytes retrieved	8.3 ± 0.4	10	13
% maturity of COC[b]	48.4 ± 2.3	40	46.2
% fertilization	57.2±2.3	10	15.4
% development[c]	32.5±2.3	0	0
% pregnancy	17.0	–	–

Note: COC = cumulus–oocyte complex. Values are means ± SEM. Data are obtained from 176 patients unless described.

[a] One hMG ampoule containts 75 IU.

[b] Percentage of mature COC evaluated by morphology.

[c] Percentage of oocytes developed to eight-cell stage or later at Day 3 post-IVF/intracytoplasmic sperm injection.

[d] Representative samples were selected from 50 male factor patients for GST expression profiling. The averaged age of 50 male factor patients was 35.2 ± 0.8 years old.

Ito. GSTT1 as a marker for age-related infertility. Fertil Steril 2007.

FIGURE 1

Up-regulation of GSTT1 in granulosa cells with aging. (**A**) Relative expression of GST isoform mRNA in representative mural granulosa cells from young (28 years) and older (36 years) male factor patients. The difference in the expression of each GST mRNA is shown as the mean log of fold increase with SEM from three independent experiments. (**B**) Correlation between GSTT1 mRNA expression in mural granulosa cells from male factor patients and the age of the patients (N = 43). Statistical analysis was conducted using Pearson's correlation contingence ($r = 0.36$, $P<.05$). (**C, D**) Immunostaining of GSTT1 protein (red) in mural (**C**) and cumulus (**D**) granulosa cells. *Left panels* show typical microphotographs from young (**C**: 25 years, **D**: 28 years) and older (**C**: 38 years, **D**: 38 years) patients. The cells were counterstained with Hoechst 33342 at 10 μM to visualize the nuclei (blue). *Right panels* show the mean fluorescence intensity of GSTT1 per cell with SEM from young (**C**: N = 9, 25–34 years, **D**: N = 7, 25–34 years) and older (**C**: N = 12, 38–43 years, **D**: N = 5, 37–42 years) patients. The data were analyzed by Student's or modified *t* test (**$P<.01$).

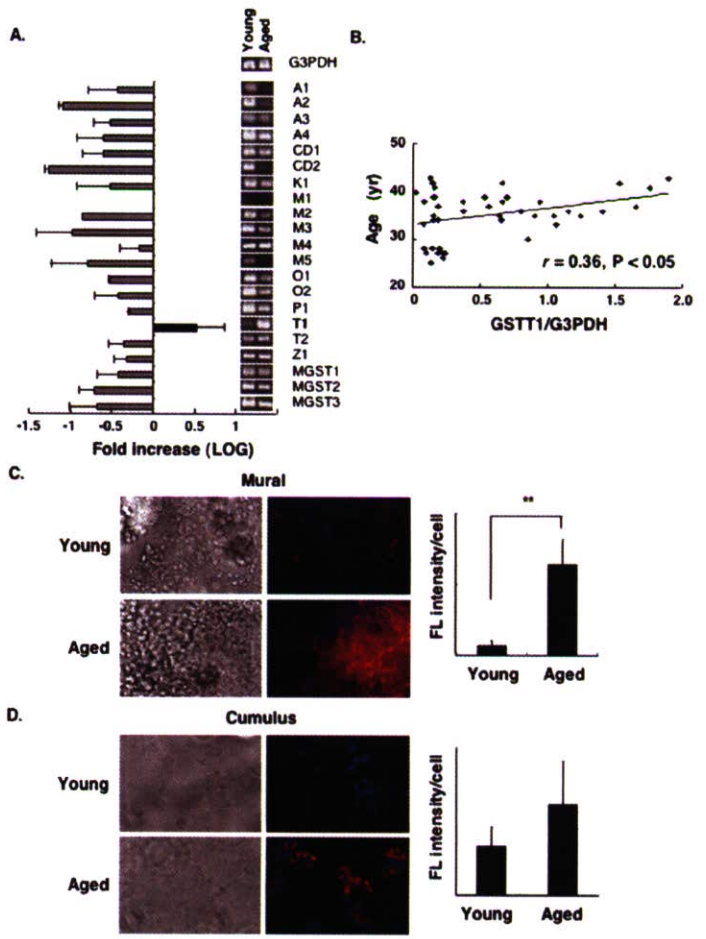

Ito. GSTT1 as a marker for age-related infertility. Fertil Steril 2007.

FIGURE 2

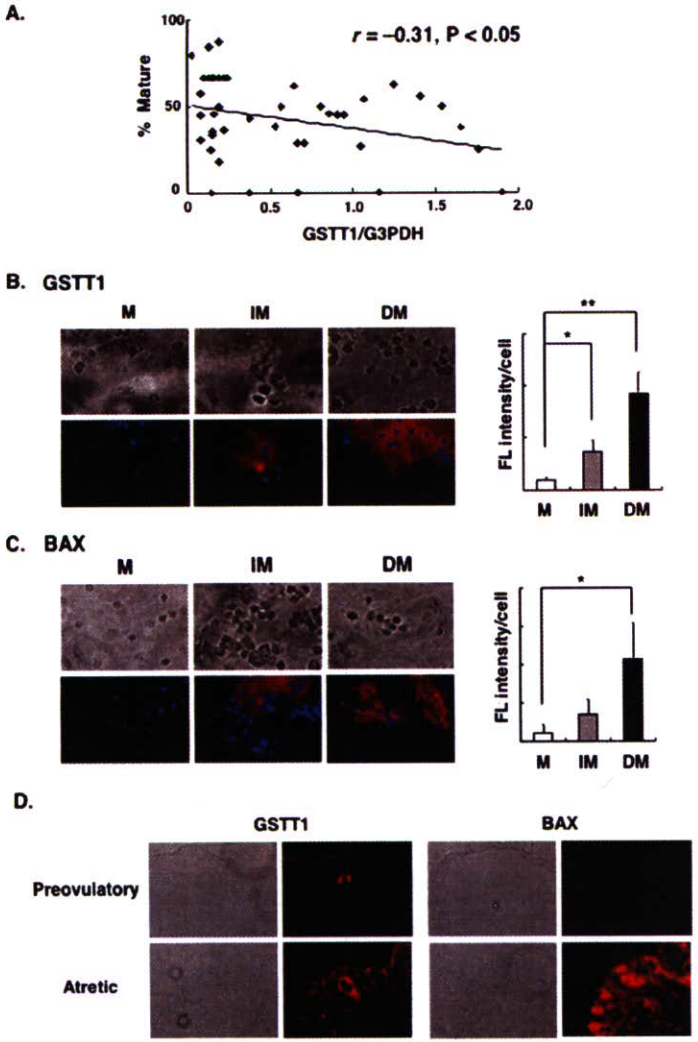

Ito. GSTT1 as a marker for age-related infertility. Fertil Steril 2007.

FIGURE 2 CONTINUED

Relationship between GSTT1 and COC maturity. (**A**) Correlation between GSTT1 mRNA expression in mural granulosa cells from male factor patients and frequency of mature COCs (N = 43). Statistical analysis was conducted using Pearson's correlation contingence ($r = -0.31$, $^*P<.05$). (**B, C**) Immunostaining of GSTT1 (**B**) and BAX (**C**) (red) in cumulus cells from male factor patients. *Left panels* show typical microphotographs of cumulus cells from mature (M), immature (IM), and dysmature (DM) COCs from a male factor patient (**B**: 35 years, **C**: 35 years). The cells were counterstained with Hoechst 33342 at 10 μM to visualize the nuclei (blue). *Right panels* show the mean fluorescence intensity of GSTT1 and BAX per cell with SEM from male factor patients (N = 5, 33–38 years). The data were analyzed by Student's or modified *t* test ($^*P<.05$, $^{**}P<.01$). (**D**) Immunostaining of GSTT1 and BAX in mouse preovulatory (8 hours post-hCG injection) and atretic follicles (72 hours post-PMSG injection).

FIGURE 3

Relationship between GSTT1 expression and oocyte quality in other factor patients. (**A**) Correlation between GSTT1 mRNA expression in mural granulosa cells from tubal and unknown factor patients and frequency of mature COCs or frequency of developmental capacity to the eight-cell stage (N = 126). Statistical analysis was conducted using Pearson's correlation contingence (not significant). (**B, C**) Frequency of mature COCs and developmental capacity of oocytes to eight-cell stage from tubal and unknown factor patients. GSTT1/G3PDH >1.0 (**B**, N = 17) or 1.1 (**C**, N = 14) was regarded as the high group and <0.2 (N = 25) as the low group. Those groups were compared statistically using Student's *t* test ($^*P<.05$, $^{**}P<.01$). Data are shown as the mean with SEM.

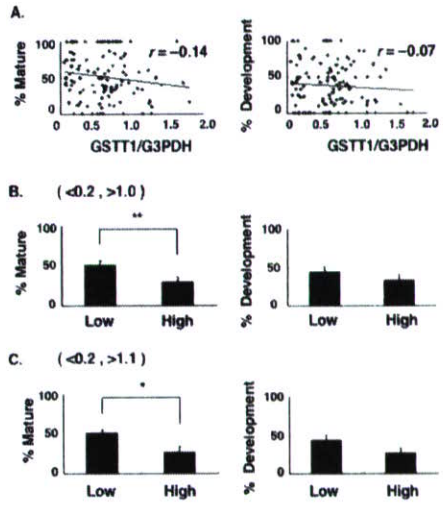

Ito. GSTT1 as a marker for age-related infertility. Fertil Steril 2007.

selected samples, the developmental capacity of oocytes from the patients with low GSTT1 was likely to be higher than that in the patients with high GSTT1 (Fig. 3B; low: 43.9%; high: 33.1%), although it was not significantly different (P=.3). The tendency was more apparent when high expression of GSTT1 was set at >1.1 GSTT1/G3PDH (Fig. 3C; COC maturity: low 51.3 %, N = 25; high 27.2%, N = 14, P<.05; developmental capacity: low 43.9 %; high 26.4%, P=.09). These results suggest that the definition of an optimal threshold of GSTT1 level may be useful for the diagnosis of age-related infertility.

FSH and Oxidative Stress as Inducers of GSTT1 in KGN Granulosa-Like Tumor Cells

In the process of aging, the serum concentration of gonadotropins such as FSH and LH is elevated (23). Thus, expression of GSTT1 in granulosa cells might be regulated by elevated gonadotropins. To examine this possibility, expression of GSTT1 in KGN cells stimulated with FSH, LH, and hCG was analyzed by immunostaining. FSH increased the expression of GSTT1, even at 0.5 ng/mL (Fig. 4A; P<.05), whereas LH and hCG did not (Fig. 4B, C). These results indicate that FSH could promote GSTT1 expression in granulosa cells. We next studied whether GSTT1 was up-regulated by oxidative stress in vitro, because oxidative stress is a major aging factor. When KGN cells were stimulated with H_2O_2 at 10 μM, GSTT1 was significantly up-regulated in a time-dependent manner (Fig. 4D; about 4.5-fold increase at 24 hours, P<.001), suggesting that oxidative stress was involved in the up-regulation of GSTT1. Taking these results together, our study supports the notion that GSTT1 is up-regulated by aging in granulosa cells and could be used as a biomarker for age-related infertility.

DISCUSSION

Reactive oxygen species and antioxidants are in balance in a young and healthy body; however, overabundance of ROS because of dysfunction of antioxidants during aging influences the reproductive life span of a woman (6). In fact, granulosa cells from older patients expressed less SOD1, SOD2, and catalase than those from young patients, and contained defective mitochondria (24). In addition, follicular fluid from older women exhibited decreased expression of GSTP and reduced activities of glutathione transferase and catalase (25). Although it is uncertain whether antioxidant systems are completely defective in aged reproductive cells, disorders of several molecules must be involved in accelerating reproductive aging.

GSTs are functionally versatile proteins. In addition to their function in catalyzing the conjugation of genotoxins to glutathione (GSH), peroxidase and isomerase activities have been reported. GSTs can also inhibit Jun N-terminal

FIGURE 4

Expression of GSTT1 in KGN cells treated with various stimuli. KGN cells were treated with recombinant human FSH (**A**), human LH (**B**), and hCG (**C**) at the indicated concentration for 12 hours, and with H_2O_2 at 10 μM for the indicated duration (**D**). The integrated fluorescence intensity of GSTT1 was measured and normalized with the number of cells. Data are shown as the mean fluorescence intensity per cell with SEM. Statistical analysis was conducted using one-way analysis of variance (**A**, $P<.05$; **D**, $P<.001$) followed with Student's *t* test (*$P<.05$, **$P<.01$, ***$P<.001$).

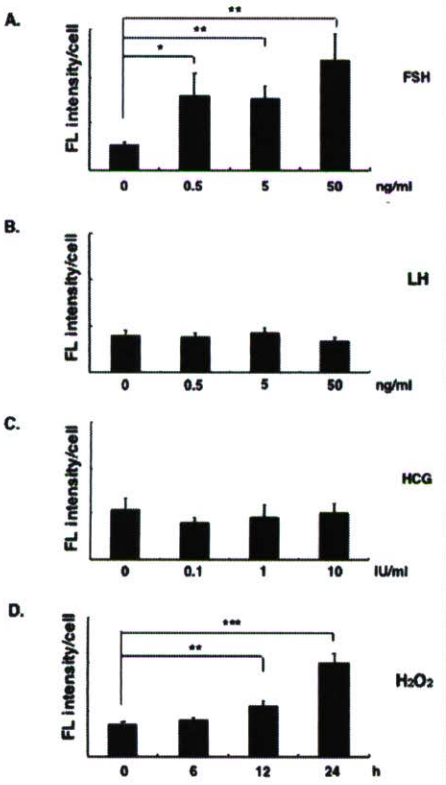

Ito. GSTT1 as a marker for age-related infertility. Fertil Steril 2007.

kinase, resulting in protection of cells against H_2O_2-induced cell death (26). In general, aging causes cellular dysfunction and apoptosis via loss of antioxidants; thus, GSTs are expected to be down-regulated by aging. In this study, GSTs, except for GSTT1, were down-regulated by aging in mural granulosa cells, although further analysis is required. It is of interest that GSTT1 could not bind to GSH-agarose or S-hexyl-GSH-agarose, unlike the other GSTs (27). GSTT1 has been reported to have conflicting properties, showing detoxification activity and production of a genotoxic metabolite (28). Therefore, the mechanism of expression of GSTT1 might be completely different from that of the other GSTs.

The information obtained from cumulus cells is important in predicting oocyte quality. Several indicators of oocyte quality have been reported using cumulus cells from infertile patients. For example, the abundance of pentraxin 3, a hyaluronan stabilizer, in cumulus cells was associated with the integrity of embryos leading to pregnancy (29). Similarly, cyclooxygenase, hyaluronic acid synthase 2, and gremlin were highly expressed in cumulus cells detached from oocytes scored as high grade (30). Reduced expression of progesterone receptors in cumulus cells was correlated with good embryo quality (31). Although the morphology of COCs was not associated with the nuclear maturity of oocytes (32, 33), our results showing a negative correlation between GSTT1 expression and COC maturity led to the idea that COC maturity might be consistent with the apoptotic status of cumulus cells. The apoptotic status of granulosa cells is altered with age (34), and correlates negatively with oocyte quality (8). In this context, the reported function of BAX in the acceleration of follicle atresia (35) and the expression pattern of BAX in cumulus cells in this study suggest that insufficiently mature COCs might be isolated from follicles towards atresia. Up-regulation of GSTT1 in granulosa cells might therefore be a response to apoptosis.

Diagnostic evaluation of oocyte quality is of clinical importance in achieving a successful pregnancy. Although morphologic evaluation of COCs can be useful as a first approach to the selection of oocytes of high quality, the second approach should use biomarkers. In this context, GSTT1 must be a predictor of both aging and oocyte quality. Although GSTT1 expression in the samples from tubal and unknown factor patients did not correlate with COC maturity, extraction of samples based on GSTT1 expression level gave an insight into the diagnosis of age-related infertility. A negative correlation between GSTT1 and COC maturity was observed in the selected granulosa cells from the tubal and unknown factor patients. Furthermore, the developmental capacity of oocytes from the selected patients with low GSTT1 was likely to be higher than that with high GSTT1. In this study, GSTT1 threshold was set at GSTT1/G3PDH >1 or 1.1 for high expression and GSTT1/G3PDH <0.2 for low expression to extract the aging factor from all other infertility factors. Because the mild selection of patients (e.g., <0.3 as low and >0.7 as high) did result in correlation with neither COC maturity nor developmental capacity (data not shown), a more severe selection seems to be more applicable for diagnosis of the aging factor. Although the additional biomarkers for oocyte quality might support the diagnosis, the GSTT1 level in granulosa cells could be a good indicator for age-related infertility.

The serum concentration of FSH and LH is known to increase gradually during aging (23). These changes in the ovarian micromilieu might affect the expression of downstream molecules. In our in vitro model, FSH appeared to induce GSTT1 expression. Interestingly, FSH is thought to act as an antiapoptotic molecule in ovaries and granulosa cells by increasing GSH (10, 36). A genetic and longitudinal study revealed that GSTT1 polymorphisms influence mortality in the elderly (37). Notably, hCG did not increase GSTT1 expression at any of the concentrations examined, although it has also been reported to possess an antiapoptotic activity (38). Up-regulation of GSTT1 might be regarded as a self-defense response downstream of FSH signaling.

Up-regulation of GSTT1 by oxidative stress in the in vitro model system may represent a self-defense response of granulosa cells against oxidative stress. Reactive oxygen species produced by oxidative stress act as important signaling molecules, whereas excess ROS diminish cellular functions. Exogenous application of oxidative stress could therefore evoke a self-defense mechanism, although the exact molecular mechanism of GSTT1 up-regulation was uncertain. However, several reports on increased apoptosis in granulosa cells during aging conflict with the antioxidant defense theory (34, 39). This discrepancy may be explained as follows. GSTT1 in reproductive cells is induced by increased oxidative stress and FSH during aging as a self-defense mechanism; however, oxidative stress may also trigger polymorphisms of GSTT1. As a result, overexpression of mutated GSTT1 (nonfunctional) could not rescue the cells. Further studies should be undertaken to evaluate this possibility.

In conclusion, the present study strongly suggests that GSTT1 in mural and cumulus granulosa cells is a possible indicator of aging of granulosa cells and oocytes. Both FSH and oxidative stress up-regulated GSTT1 in the granulosa cell line, supporting the notion that GSTT1 is a marker of aging. Notably, up-regulation of GSTT1 protein was related to the expression of BAX in cumulus cells classified as immature or dysmature, suggesting that the apoptotic status of cumulus cells is associated with the expression of GSTT1. Age-related decline of oocyte quality could be associated with oxidative stress-induced apoptosis defined by GSTT1 up-regulation.

Acknowledgments: We thank Mr. Junwen Qin at the University of Tokyo for his technical support.

REFERENCES

1. Baird DT, Collins J, Egozcue J, Evers LH, Gianaroli L, Leridon H, et al. Fertility and ageing. Hum Reprod Update 2005;11:261–76.
2. Burwinkel TH, Buster JE, Scoggan JL, Carson SA. Basal follicle stimulating hormone (FSH) predicts response to controlled ovarian hyperstimulation (COH)-intrauterine insemination (IUI) therapy. J Assist Reprod Genet 1994;11:24–7.
3. te Velde ER, Scheffer GJ, Dorland M, Broekmans FJ, Fauser BC. Developmental and endocrine aspects of normal ovarian aging. Mol Cell Endocrinol 1998;145:67–73.
4. Pellestor F, Anahory T, Hamamah S. Effect of maternal age on the frequency of cytogenetic abnormalities in human oocytes. Cytogenet Genome Res 2005;111:206–12.
5. Linnane AW, Zhang C, Baumer A, Nagley P. Mitochondrial DNA mutation and the ageing process: bioenergy and pharmacological intervention. Mutat Res 1992;275:195–208.
6. Agarwal A, Gupta S, Sharma RK. Role of oxidative stress in female reproduction. Reprod Biol Endocrinol 2005;3:28.
7. Chao HT, Lee SY, Lee HM, Liao TL, Wei YH, Kao SH. Repeated ovarian stimulations induce oxidative damage and mitochondrial DNA mutations in mouse ovaries. Ann N Y Acad Sci 2005;1042:148–56.
8. Seino T, Saito H, Kaneko T, Takahashi T, Kawachiya S, Kurachi H. Eight-hydroxy-2'-deoxyguanosine in granulosa cells is correlated with the quality of oocytes and embryos in an in vitro fertilization-embryo transfer program. Fertil Steril 2002;77:1184–90.
9. Das S, Chattopadhyay R, Ghosh S, Ghosh S, Goswami SK, Chakravarty BN, et al. Reactive oxygen species level in follicular fluid—embryo quality marker in IVF? Hum Reprod 2006;21:2403–7.
10. Tsai-Turton M, Luderer U. Opposing effects of glutathione depletion and follicle-stimulating hormone on reactive oxygen species and apoptosis in cultured preovulatory rat follicles. Endocrinology 2006;147:1224–36.
11. Nakahara K, Saito H, Saito T, Ito M, Ohta N, Takahashi T, et al. The incidence of apoptotic bodies in membrana granulosa can predict prognosis of ova from patients participating in in vitro fertilization programs. Fertil Steril 1997;68:312–7.
12. Nakahara K, Saito H, Saito T, Ito M, Ohta N, Takahashi T, et al. Ovarian fecundity in patients with endometriosis can be estimated by the incidence of apoptotic bodies. Fertil Steril 1998;69:931–5.
13. Mari M, Cederbaum AI. Induction of catalase, alpha, and microsomal glutathione S-transferase in CYP2E1 overexpressing HepG2 cells and protection against short-term oxidative stress. Hepatology 2001;33:652–61.
14. Deakin M, Elder J, Hendrickse C, Peckham D, Baldwin D, Pantin C, et al. Glutathione S-transferase GSTT1 genotypes and susceptibility to cancer: studies of interactions with GSTM1 in lung, oral, gastric and colorectal cancers. Carcinogenesis 1996;17:881–4.
15. Strange RC, Fryer AA. The glutathione S-transferases: influence of polymorphism on cancer susceptibility. IARC Sci Publ 1999;231–49.
16. Spurdle AB, Webb PM, Purdie DM, Chen X, Green A, Chenevix-Trench G. Polymorphisms at the glutathione S-transferase GSTM1, GSTT1 and GSTP1 loci: risk of ovarian cancer by histological subtype. Carcinogenesis 2001;22:67–72.
17. Seidegard J, Vorachek WR, Pero RW, Pearson WR. Hereditary differences in the expression of the human glutathione transferase active on trans-stilbene oxide are due tobecause of a gene deletion. Proc Natl Acad Sci USA 1988;85:7293–7.
18. Taningher M, Malacarne D, Izzotti A, Ugolini D, Parodi S. Drug metabolism polymorphisms as modulators of cancer susceptibility. Mutat Res 1999;436:227–61.
19. Wilson MH, Grant PJ, Hardie LJ, Wild CP. Glutathione S-transferase M1 null genotype is associated with a decreased risk of myocardial infarction. FASEB J 2000;14:791–6.
20. Sata F, Yamada H, Kondo T, Gong Y, Tozaki S, Kobashi G, et al. Glutathione S-transferase M1 and T1 polymorphisms and the risk of recurrent pregnancy loss. Mol Hum Reprod 2003;9:165–9.
21. Babu KA, Rao KL, Kanakavalli MK, Suryanarayana VV, Deenadayal M, Singh L. CYP1A1, GSTM1 and GSTT1 genetic polymorphism is associated with susceptibility to polycystic ovaries in South Indian women. Reprod Biomed Online 2004;9:194–200.
22. Nishi Y, Yanase T, Mu Y, Oba K, Ichino I, Saito M, et al. Establishment and characterization of a steroidogenic human granulosa-like tumor cell line, KGN, that expresses functional follicle-stimulating hormone receptor. Endocrinology 2001;142:437–45.
23. Klein NA, Battaglia DE, Fujimoto VY, Davis GS, Bremner WJ, Soules MR. Reproductive aging: accelerated ovarian follicular development associated with a monotropic follicle-stimulating hormone rise in normal older women. J Clin Endocrinol Metab 1996;81:1038–45.
24. Tatone C, Carbone MC, Falone S, Aimola P, Giardinelli A, Caserta D, et al. Age-dependent changes in the expression of superoxide dismutases

and catalase are associated with ultrastructural modifications in human granulosa cells. Mol Hum Reprod 2006;12:655–60.
25. Carbone MC, Tatone C, Delle Monache S, Marci R, Caserta D, Colonna R, et al. Antioxidant enzymatic defences in human follicular fluid: characterization and age-dependent changes. Mol Hum Reprod 2003;9:639–43.
26. Sheehan D, Meade G, Foley VM, Dowd CA. Structure, function and evolution of glutathione transferases: implications for classification of non-mammalian members of an ancient enzyme superfamily. Biochem J 2001;360:1–16.
27. Harris JM, Meyer DJ, Coles B, Ketherer B. A novel glutathione transferase (13-13) isolated from the matrix of rat liver mitochondria having structural similarity to class theta enzymes. Biochem J 1991;278:137–41.
28. Thier R, Pemble SE, Kramer H, Taylor JB, Guengerich FP, Ketterer B. Human glutathione S-transferase T1-1 enhances mutagenicity of 1,2-dibromoethane, dibromomethane and 1,2,3,4-diepoxybutane in *Salmonella typhimurium*. Carcinogenesis 1996;17:163–6.
29. Zhang X, Jafari N, Barnes RB, Confino E, Milad M, Kazer RR. Studies of gene expression in human cumulus cells indicate pentraxin 3 as a possible marker for oocyte quality. Fertil Steril 2005;83(Suppl 1):1169–79.
30. McKenzie LJ, Pangas SA, Carson SA, Kovanci E, Cisneros P, Buster JE, et al. Human cumulus granulosa cell gene expression: a predictor of fertilization and embryo selection in women undergoing IVF. Hum Reprod 2004;19:2869–74.
31. Hasegawa J, Yanaihara A, Iwasaki S, Otsuka Y, Negishi M, Akahane T, et al. Reduction of progesterone receptor expression in human cumulus cells at the time of oocyte collection during IVF is associated with good embryo quality. Hum Reprod 2005;20:2194–200.
32. Hammitt DG, Syrop CH, Van Voorhis BJ, Walker DL, Miller TM, Barud KM. Maturational asynchrony between oocyte cumulus–coronal morphology and nuclear maturity in gonadotropin-releasing hormone agonist stimulations. Fertil Steril 1993;59:375–81.
33. Rattanachaiyanont M, Leader A, Leveille MC. Lack of correlation between oocyte–corona–cumulus complex morphology and nuclear maturity of oocytes collected in stimulated cycles for intracytoplasmic sperm injection. Fertil Steril 1999;71:937–40.
34. Sadraie SH, Saito H, Kaneko T, Saito T, Hiroi M. Effects of aging on ovarian fecundity in terms of the incidence of apoptotic granulosa cells. J Assist Reprod Genet 2000;17:168–73.
35. Perez GI, Robles R, Knudson CM, Flaws JA, Korsmeyer SJ, Tilly JL. Prolongation of ovarian lifespan into advanced chronological age by Bax-deficiency. Nat Genet 1999;21:200–3.
36. Tilly JL, Tilly KI. Inhibitors of oxidative stress mimic the ability of follicle-stimulating hormone to suppress apoptosis in cultured rat ovarian follicles. Endocrinology 1995;136:242–52.
37. Christiansen L, Brasch-Andersen C, Bathum L, Kruse TA, Christensen K. A longitudinal study of the effect of GSTT1 and GSTM1 gene copy number on survival. Mech Ageing Dev 2006;127:597–9.
38. Matsubara H, Ikuta K, Ozaki Y, Suzuki Y, Suzuki N, Sato T, et al. Gonadotropins and cytokines affect luteal function through control of apoptosis in human luteinized granulosa cells. J Clin Endocrinol Metab 2000;85:1620–6.
39. Vaskivuo TE, Anttonen M, Herva R, Billig H, Dorland M, te Velde ER, et al. Survival of human ovarian follicles from fetal to adult life: apoptosis, apoptosis-related proteins, and transcription factor GATA-4. J Clin Endocrinol Metab 2001;86:3421–9.